SEDIMENTOLOGY the journal of the International Association of Sedimentologists

Sedimentology (2019) doi: 10.1111/sed.12662

An extreme wave event in eastern Yucatán, Mexico: Evidence of a palaeotsunami event during the Mayan times

JAVIER LARIO*, CHRIS SPENCER†, TERESA BARDAJÍ‡, ÁNGEL MARCHANTE§, VICTOR H. GARDUÑO-MONROY¶, JORGE MACIAS** and SERGIO ORTEGA††

**Facultad de Ciencias, UNED, Madrid, 28040, Spain (E-mail: javier.lario@ccia.uned.es)*

†Department of Geography and Environmental Management, University of the West England, Bristol, BS16 1QY, UK

‡Departamento de Geología, Geografía y Medio Ambiente, Universidad de Alcalá, Plaza de San Diego, Madrid, 28801, Spain

§Grupo de Investigación TARHA, Universidad de las Palmas de Gran Canaria, Las Palmas, 35001, Spain

¶Departamento de Geología y Mineralogía, Universidad Michoacana de San Nicolás de Hidalgo, Morelia, Michoacán, 58004, Mexico

***Departamento de A.M., E. e I.O. y Matemática Aplicada, Facultad de Ciencias, Universidad de Málaga, Málaga, 29016, Spain*

††Laboratorio de Métodos Numéricos, SCAI, Universidad de Málaga, Málaga, 29016, Spain

Associate Editor – César Andrade

ABSTRACT

The Yucatán Peninsula, Mexico, has typically been considered a tectonically stable region with little significant seismic activity. The region though, is one that is regularly affected by hurricanes. A detailed survey of *ca* 100 km of the eastern Yucatán and Cozumel coast identified the presence of ridges containing individual boulders measuring >1 m in length. The boulder ridges reach 5 m in height and their origin is associated with extreme wave event activity. Previously modelled tsunami waves from known seismically active zones in the region (Muertos Thrust Belt and South Caribbean Deformed Belt) are not of sufficient scale in the area of the Yucatán Peninsula to have produced the boulder ridges recorded in this study. The occurrence of hurricanes in this region is more common, but two of the most destructive (Hurricane Gilbert 1988 and Hurricane Wilma 2005) produced coastal waves too small to have created the ridges recorded here. In this paper, a new tsunami model with a source area located on the Motagua/Swan Island Fault System has been generated that indicates a tsunami event may have caused the extreme wave events that resulted in the deposition of the boulder ridges.

Keywords Boulders, extreme wave event, palaeoseismology, tsunami.

INTRODUCTION

The Yucatán Peninsula of Mexico is a carbonate platform composed of Eocene-age limestone in the interior, with offlapping sequences corresponding to a Quaternary coastline (Weidie, 1985). The present-day coastline is incised into the Pleistocene shelf margin, reef and back-reef limestones, which were deposited during the last interglacial sea-level highstand (marine isotopic stage – MIS – 5). The Pleistocene deposits extend inland for some 10 km and form the most recent of a sequence of accreted carbonate units reaching at least 12 m in thickness (Ward,

1985). These deposits are present as two reef tracts up to 3 metres above sea-level (m a.s.l.) and 6 m a.s.l., and Th/U dating confirms that the reef tracts are contemporary and formed during Marine Isotope Stage 5e (Blanchon *et al.*, 2009). The peninsula is considered to have been tectonically stable since the late Pleistocene (Szabo *et al.*, 1978); this belief is also supported by the lack of recorded historical seismicity (Márquez-Azua *et al.*, 2004).

A detailed survey of *ca* 100 km of the eastern Yucatán coast (Quintana Roo and Cozumel Island) identified the presence of beach ridges comprised of individual boulders measuring >1 m in length (Fig. 1). The ridges reach 5 m in height and their origin is inferred to be associated with extreme wave event (EWE) activity, associated with either tsunamis (not recorded as having occurred in the area) or hurricanes (frequently recorded in the area). Recently, these boulder ridges were partially described by Shaw & Benson (2015) and attributed to a tsunami event, but no evidence of the tsunami source was provided.

BOULDER RIDGES DESCRIPTION

There are two main areas where boulder ridges were studied in detail. One is along the coast in Quintana Roo between Playa del Carmen and Caleta Tankah and the other area is located on the eastern coast of Cozumel Island (Fig. 1).

The ridges are composed of accumulations of coral reef boulders, with most being angular in shape and imbricated. Individual boulders are more than 1 m long and the ridges reach heights of 5 m. Accumulations of boulders are more extensive along rockier sections of the coast, rocky platforms and capes, while in *caletas* (karstic bays) boulder ridges are absent and replaced by a ridge of sand, reef pebbles and cobbles. Typically, the boulders originate from joint bounded blocks (JBB) originally forming part of the late Pleistocene platforms near mean sea-level (m.s.l.), corresponding to MIS 5e (Blanchon *et al.*, 2009). At some of the sites a second smaller ridge exists overlapping the main one, the smaller ridge being typically composed of pebbles and cobbles.

Methodology

The area has been divided into a series of sectors in order to complete surveys of the ridges. In this area the late interglacial marine sediments extend, consisting of two separate linear reef tracts that are offset and at different elevations (Blanchon *et al.*, 2009). Holocene ridges and beaches overlie the lower reef tract that crops out along the northern shore for 500 m inland of the reef crest outcrop from below mean sea-level to +3 m. The crest is composed of large *A. palmate* colonies dispersed within an *A. palmate* boulder gravel; this is flanked by a reef front with a mixed coral assemblage and a large, lagoonal patch-reef complex (Blanchon

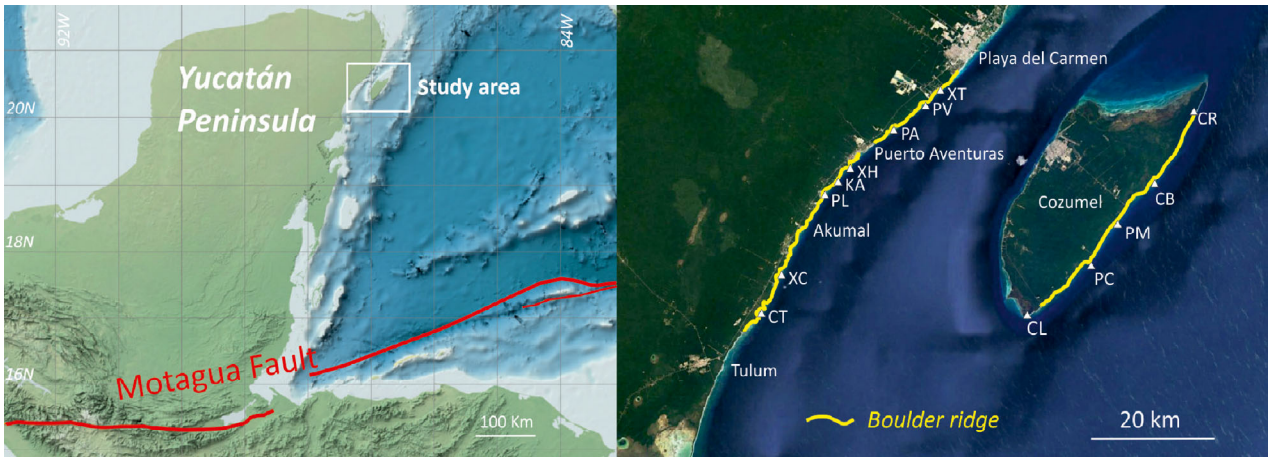

Fig. 1. Location maps showing position of the study area in the Yucatán Peninsula and sites with boulder ridges. Sites are: XT – Xcaret; PV – Punta Venado; PA – Paamul; XH – Xpu Ha; KA – Kantenah; PL – Palladium Resort; XC – Xcacel; CT – Caleta Tankah Cozumel; CR – Castillo Real; CB – Coco′s Beach; PM – Punta Morena; PC – Punta Chiqueros; CL – Celarain Lighthouse.

et al., 2009). Geomorphologically these features correspond to a marine platform developing between 0·5 m a.s.l. and 1·0 m a.s.l. in some of the sectors and was fractured in a JBB (joint bound boulder) pattern.

In each sector, where a boulder ridge was present, several boulders have been measured and the most representative (largest or highest) have been included in Table 1. In total, more than 100 boulders were measured [a, b and c axis dimensions, height, distance to the coastline (d) and the main lithology]. Measurements were taken using non-deformable metric tapes and a Leica Disto X310 laser distance measurer (Leica, Wetzlar, Germany). Pictures of the boulders were ground-based, taken with a Canon Powershot SX240HS camera (Canon, Tokyo, Japan) and processed for photogrammetry using Agisoft Photoscan software (Agisoft, 2017). As a result of the photogrammetry, a three-dimensional reconstruction of the boulders was created and all of the dimensions calculated. Thus, the volume of these boulders can be measured accurately (Fig. 2). The blocks and boulders represent heterogeneous reef-rock and consist of varying percentages of several different lithofacies.

Ridge descriptions

Descriptions of different sectors of boulder ridges are found below. These sectors occur from Playa del Carmen to Cozumel Island.

Playa del Carmen–Xcaret (XC)
Southward of Playa del Carmen (southern Playacar residential development), a ridge of imbricated boulders can be seen reaching up to 4·5 to 5·0 m a.s.l. The largest boulders are at the bottom of the ridge, with imbricated boulders present at the top of the ridge. The ridge continues on to Xcaret Park (XT). Mayan ruins exist in the park (Xcaret archaeological site), and to the north a single structure facing the sea and referred to as K-1 by Andrews & Andrews (1975) has been identified and dated as a temple from the Post-Classic Mayan period. The temple rests on a platform of large boulders, a setting that was previously described during studies performed in 1986 and 1987 by Con (1991) indicating that this setting is not an artefact of recent restoration work (Fig. 3).

Paamul (PA)
Paamul beach is a small sandy bay without boulders. Southward of the bay a boulder ridge is present, formed of late interglacial reef deposits. The ridge develops in elevation from 0·5 to 4·0 m a.s.l., with its lower section closer to the coastline (1·8 to 2·0 m from the coastline) and the higher section at a greater distance (31 m). The late Pleistocene marine platform is present across the whole area and is highly fractured. This is the source of the boulders that form the ridges. To the south at 1·20 m a.s.l. a microcliff is present in the late Pleistocene deposits and accumulations of reef pebbles and cobbles occur attached to the seaward side of the boulder ridge. The boulder ridge, however, disappears at Hard Rock Hotel (Puerto Aventuras) where the coast is highly modified by tourist infrastructure (Fig. 4).

Xpu Ha (XH)
To the south (Punta Chile) no ridge is present at the beach. However, a ridge can be seen some metres further along the coast. This ridge reaches up to 4 to 5 m a.s.l. and consists of reef cobbles at the top and angular boulders at the bottom. The marine platform is quite narrow here [distance *(d)* = 2 m] and to the north there is a sandy beach with no visible ridge.

Palladium (PL) – Caleta Kantenah (KA)
The Palladium (PL) sector is located around the Gran Palladium Resort. Just in front of the resort there is a small embayment (Caleta Kantenah) with no ridge present. To the south a small ridge is present with some reef cobbles that contain imbricated boulders throughout reaching 4 m a.s.l. on average and a distance to the coastline of 10 to 12 m. Details of the deposits are presented in Fig. 5. The ridge extends inland up to 50 m with smaller scattered boulders and rounded cobbles. The maximum height of the ridge is 6 m a.s.l. and the ridge terminates at the Dolphin Discovery Center.

To the north of the Dolphin Discovery Center a ridge is present that contains reef cobbles with pebbles on top (1 m a.s.l.) and boulders at the bottom. The ridge reaches up to 4·5 m a.s.l. and is situated over a late Pleistocene marine platform with a distance to the coastline of 22 to 32 m and fractured in a JBB pattern. The sector terminates at the Xpu Ha sector (Punta Chile, XH).

Within this ridge, towards the top there are Mayan ruins named 'La Ruina' (Fig. 6). There is no evidence of boulders resting on the archaeological remains indicating that the ridge was already *in situ* before construction of this

Table 1. Minimum height of the extreme wave (tsunami and storm) necessary to move the boulders listed.

							Nott, 2003 – JBB		Engel & May, 2012 – JBB	
Sector	Boulder	a (m)	b (m)	c (m)	Corrected vol. (m^3)	Weight kg	Ht (m)	Hs (m)	Ht (m)	Hs (m)
Paamul	BPM1	1·89	1·39	0·51	0·66	1490	1·0	4·0	1·2	4·9
	BPM2	1·19	0·46	0·46	0·12	280	0·1	0·6	1·1	4·4
	BPM3	1·37	0·81	0·45	0·24	555	0·4	1·7	1·1	4·3
	BPM5	0·84	0·80	0·70	0·23	523	0·3	1·0	1·7	6·7
	BPM6	1·48	1·14	0·74	0·61	1389	0·5	2·0	1·8	7·1
	BPM7	1·72	0·82	0·49	0·34	769	0·4	1·6	1·2	4·7
	BPM8	1·57	0·98	0·55	0·41	941	0·5	2·0	1·3	5·2
	BPM9	2·70	2·60	1·07	3·68	8355	1·6	6·5	**2·6**	**10·2**
	BPM10	3·70	1·72	0·80	2·49	5663	1·1	4·3	1·9	7·6
	B2-3	1·52	1·09	0·64	0·52	1179	0·5	2·1	1·5	6·1
	B2-4	0·85	0·77	0·53	0·17	386	0·3	1·3	1·3	5·1
	B2-5	1·26	0·90	0·58	0·32	732	0·4	1·6	1·4	5·5
	BPM11	2·00	0·74	0·57	0·41	938	0·3	1·2	1·4	5·4
Palladium-Kantenah	BPA1	1·96	0·91	0·87	0·76	1726	0·3	1·1	**2·1**	**8·3**
	BPA2	1·60	1·30	0·95	0·97	2198	0·5	2·0	**2·3**	**9·1**
	BPA3	1·84	0·93	0·77	0·65	1466	0·3	1·3	1·8	7·3
	BPA4	1·50	0·95	0·57	0·40	903	0·5	1·8	1·4	5·4
	BPA5	1·86	0·92	0·89	0·75	1694	0·3	1·1	**2·1**	8·5
	BPA7	1·10	0·55	0·50	0·15	336	0·2	0·7	1·2	4·8
	BPA8	3·90	1·45	0·57	1·58	3585	1·1	4·3	1·4	5·4
	BPA9	2·10	1·00	1·00	1·03	2336	0·3	1·2	2·4	9·5
	BPA10	2·60	1·65	1·08	2·27	5154	0·7	2·9	**2·6**	**10·3**
	BPA11	2·30	1·30	0·71	1·04	2361	0·7	2·7	1·7	6·8
	BKAN1	2·10	0·86	0·76	0·67	1527	0·3	1·2	1·8	7·3
	BKAN2	1·24	0·90	0·47	0·26	583	0·5	1·9	1·1	4·5
	BKAN4	3·10	2·01	0·70	2·14	4852	1·6	6·2	1·7	6·7
	BKAN5	2·12	1·30	0·52	0·70	1594	0·9	3·6	1·2	5·0
	BKAN8	1·21	0·78	0·41	0·19	430	0·4	1·7	1·0	3·9
	BKAN9	2·30	2·10	0·51	1·21	2740	2·0	8·1	1·2	4·9
	BKAN10	2·70	1·56	1·00	2·06	4685	0·7	2·8	**2·4**	**9·5**
Xcacel	BXC4	1·24	0·60	0·56	0·20	463	0·2	0·8	1·3	5·3
	B2	1·20	0·65	0·61	0·23	529	0·2	0·8	1·5	5·8
	B6	1·80	0·93	0·77	0·63	1434	0·3	1·3	1·8	7·3
	BA12	1·82	1·00	0·84	0·75	1700	0·4	1·4	**2·0**	**8·0**
	BN1	1·90	1·00	0·75	0·70	1585	0·4	1·6	1·8	7·2
	BN3	0·90	0·58	0·40	0·10	232	0·2	1·0	1·0	3·8
	BN5	1·40	1·17	0·76	0·61	1385	0·5	2·0	1·8	7·3
	BN6	2·02	1·20	0·42	0·50	1132	0·9	3·7	1·0	4·0
Akumal	BAK2	2·32	1·32	0·49	0·74	1669	1·0	3·9	1·2	4·7
	BAK3	2·02	1·00	0·84	0·83	1887	0·4	1·4	**2·0**	**8·0**
	BAK4	1·47	1·00	0·87	0·63	1423	0·3	1·3	**2·1**	**8·3**
	BAK5	1·30	1·24	0·38	0·30	681	1·0	4·0	0·9	3·6
	BAK6	1·38	1·02	0·86	0·59	1346	0·4	1·4	**2·1**	**8·2**
Cozumel	BCZ3	1·52	1·23	0·19	0·17	395	1·7	6·8	0·5	1·8
	BCZ4	1·44	1·19	0·32	0·27	610	1·1	4·3	0·8	3·1
	BCZ5	1·50	0·97	0·51	0·36	825	0·5	2·1	1·2	4·9
	BCZ6	3·70	2·38	0·82	3·54	8032	1·9	7·4	2·0	7·8
	BCZ7	1·90	1·60	1·20	1·79	4058	0·6	2·4	**2·9**	**11·5**
	BCZ8	2·00	1·90	0·30	0·56	1268	2·4	9·8	0·7	2·9
	BCZ9	2·49	2·00	0·70	1·71	3877	1·5	5·9	1·7	6·7

JBB, joint bounded blocks.

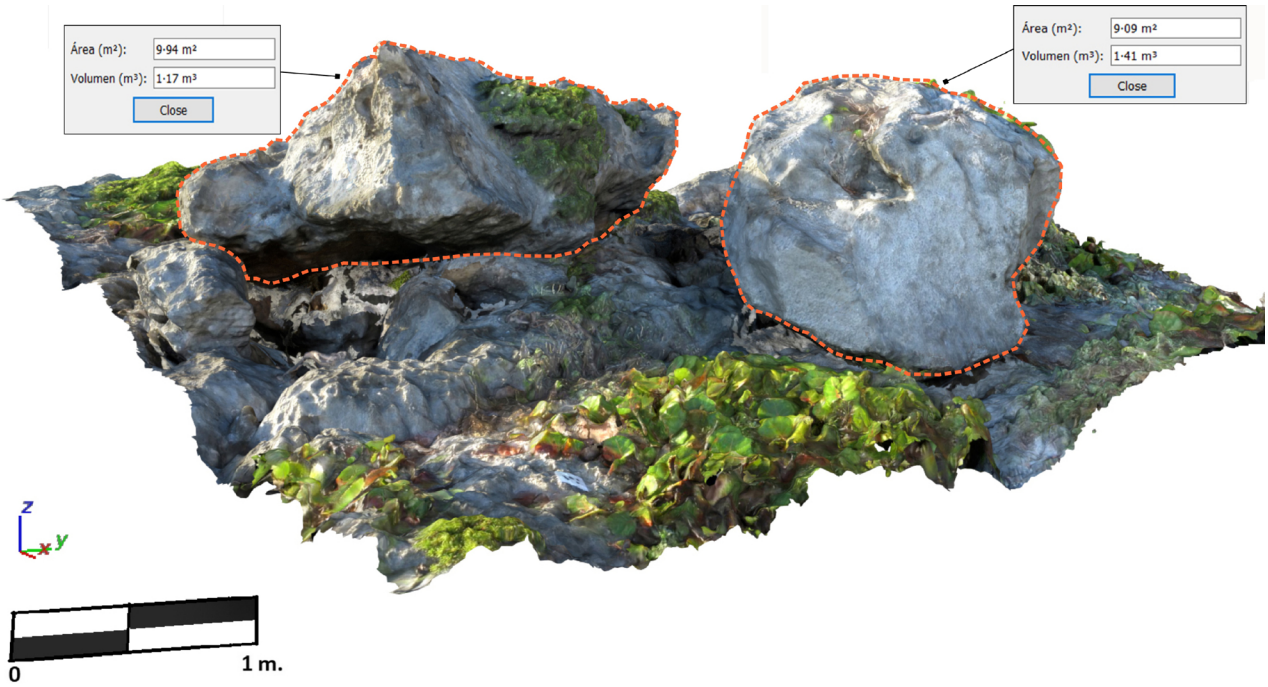

Fig. 2. Reconstructed image using Agisoft photogrammetry of boulders in the Akumal sector. All of the size attributes of boulders used in this study can be obtained from the three-dimensional reconstructions.

historical site. The ruins probably correspond to an 'adoratorio' (praying altar) from the Post-Classic Mayan period (Andrews & Andrews, 1975; Zúñiga, 2016).

Akumal

This area can be split in two sections. The first, to the south, from Casa Kukulcan-Gran Oasis Tulum to Caleta Chemuliyito is strongly affected by development resulting in extensive modifications to the coastline. Near the Gran Oasis Tulum resort there is a ridge present that reaches up to 1·5 m a.s.l. and is comprised mainly of reef cobbles and pebbles with scattered boulders on the beach. To the south the ridge reaches up to 4·5 m a.s.l. An interview with an eyewitness reported that the cobble and pebble ridges were formed during Hurricane Emily (2005) but that the boulders were not relocated during this event or by later hurricanes. In Caleta Chemuliyito, where a marine platform exists extending up to 70 m from sea, the boulder ridge rises up to 5 m a.s.l. again and its seaward side is covered by cobbles and pebbles presumably deposited during Hurricane Emily (Fig. 7).

The second section is Akumal North, a marine platform built on late Pleistocene deposits. This section is 270 m long and 65 to 70 m wide, and is overlain by clusters of imbricated boulders. From Half Moon Bay to Cenote Yal-Ku, the marine platform width narrows to 20 m and the imbricated boulder ridge is well-developed and reaching up to 4 to 5 m a.s.l. The marine platform is also fissured with a JBB pattern. The inland extent of the ridge, however, was difficult to determine because of the proliferation of residential buildings and a road that was built on top of the ridge. However, data collected in the early 1990s by Shaw & Benson (2015), shows that the inland surface of the ridge was composed of smaller boulders and cobbles that spread inland over a distance of 70 m.

Xcacel (XC)

From Xcacel beach to the south a ridge is present, composed predominantly of well-rounded cobbles and pebbles from an *A. palmata* reef and beach rock, extending up to 4·0 m a.s.l. These cobbles and pebbles rest above some single boulders from late interglacial deposits. In the Xcacelito Bay area some excavated trenches exist but no boulder ridges or cobble ridges can be observed, only sandy foredunes. At the end of Xcacelito Bay the main ridge consists of boulders reaching up to 2·5 m a.s.l. and d = 3·0 to 6·20 m. The ridge overlies a late Pleistocene marine platform (0·5 m a.s.l.) that is highly fissured in a JBB pattern. In some locations,

Fig. 3. Boulder ridge south Playa del Carmen, from south Playacar to Xcaret Park. (A) 4·5 to 5·0 m a.s.l. boulder ridge with sandy beach in front. (B) Imbricated boulders (1·35 m length) on top of narrow marine platform. (C) Post-Classic Mayan period temple (K-1) at Xcaret archaeological site associated with >1 m boulder at top of the cliff. No boulders or pebbles were found at the top or affecting the Mayan site. (D) 3·0 to 4·0 m a.s.l. boulder ridge (facing north from Xcaret temple K-1) associated with a JBB marine platform 8 to 12 m wide.

small boulders and pebbles can be found up to 23 m inland, but usually the ridge exhibits a width of 4 to 6 m. This sector ends to the south at Xel-Ha Park limits, where access was not permitted.

To the northern end of Xcacel Bay a ridge of rounded cobbles is present at $d = 15$ m. The ridge contains some boulders, composed solely of reef materials. The ridge reaches up to 5 m a.s.l. and extends up to 29 m inland. The

Fig. 4. Detailed photographs of the south Paamul sector. (A) Marine platform exhibiting fracture network (white lines) forming a JBB pattern; the arrow indicates a disaggregated boulder. (B) Boulder ridge developed up to 4·5 m a.s.l. associated with a narrow marine platform. (C) Boulder ridge up to 4·5 m a.s.l. associated with a fractured 31 m wide marine platform. (D) Rounded coral cobbles and pebbles attached to the main boulder ridge. (E) and (F) Sub-rounded imbricated coral boulders at foot of the seaward facing slope of the main ridge. JBB, joint-bound boulder.

elevation of the ridge and size of the cobbles decrease with increasing distance inland. Again, a late Pleistocene marine platform exists seaward of the ridge with an average width of 35 m to the ridge, although this width reaches 100 m at some points.

Fig. 5. Detailed photographs of the Palladium-Kantenah sector. (A) Boulder ridge up to 4 m a.s.l. associated with a marine platform. (B) Overturned reef boulder (white arrow) at the bottom of the boulder ridge. (C) Small ridge of rounded reef cobbles and pebbles related to hurricane waves that hit this coastal area over the last decade. (D) Large boulder ridge up to 4·5 m a.s.l.; note the rounded reef pebbles associated with hurricane wave activity along this coastal area over the last decade. (E) Imbricated boulders at the foot of the boulder ridge associated with a marine platform.

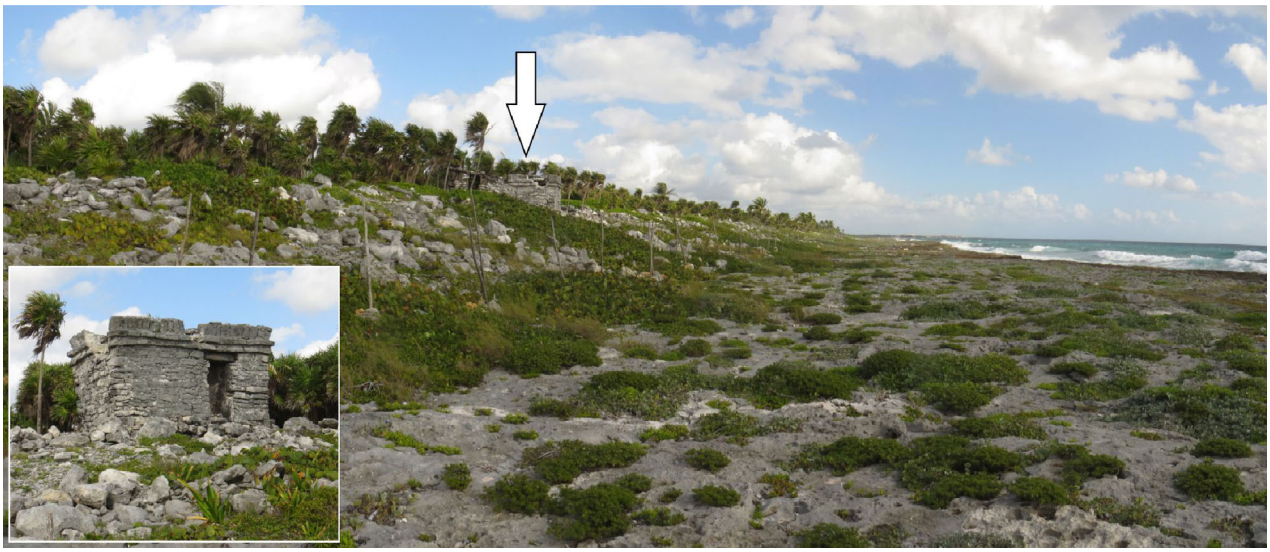

Fig. 6. Mayan ruins called 'La Ruina' sitting at 5 m a.s.l. at the top of a boulder ridge. They are interpreted as corresponding to an 'adoratorio' (praying altar) from the Post-Classic Mayan period (building height is 2·15 m).

Caleta Tankah (CT)
Surveying from Caleta Tankah to Tulum archaeological site showed that both boulder and cobble ridges are absent. There is only present a sandy beach with some associated dunes.

Cozumel Island
Boulder or cobble ridges are only present on the eastern coast of Cozumel. The survey carried out in this study only reached as far north as Coco's Beach due to access restrictions, but aerial images show that segments of the boulder ridge are present up to the vicinity of Playa Bonita-Castillo Real. Here, the boulder ridge reaches up to 3 m a.s.l. and is composed mainly of late Pleistocene calcarenites and corals with d = 3·0 to 4·5 m. The main road to the south covers much of the ridge; therefore, measurements were only taken where the boulder ridge was not affected by the road. Between Punta Morena and Punta Chiquero there is also a late interglacial rock marine platform and in this area the distance from the boulder ridge to the coast reaches 8 to 12 m. Near Faro Celarain (Celarain lighthouse) the ridge disappears, and only scattered boulders can be seen (Fig. 8).

ORIGIN OF BOULDER RIDGES

In recent years there has been discussion on coastal processes resulting in the build-up of coarse-clast ridges. Investigations along the Circum-Caribbean coastlines (Morton *et al.*, 2006, Morton *et al.*, 2008; Scheffers *et al.*, 2014) and elsewhere (Etienne *et al.*, 2011; Richmond *et al.*, 2011) have reinforced the view that coarse-clast ridges backing tropical reef settings result from the periodic impact of storm waves. Previous research completed by some of these authors (Scheffers *et al.*, 2009) in their studies of storm/tsunami deposits in the Caribbean indicated that the problems of coastal coarse sediment transport, in particular the transport of large boulders by waves, are far from being solved, and their discussion is highly controversial among field scientists and modellers. In their list of the main diagnostic features discriminating between storm induced and tsunamigenic coarse deposits, these authors concluded that boulder rampart/ridges formed by tsunamis include: boulders of over 300 tons; mega-clasts diminishing in size landward; a seaward strip of bare rock; imbrication strongly present; presence of seaward slopes and a smooth landward slope or boulders, mostly angular.

Mastronuzzi *et al.* (2007) argued that the use of boulder accumulations as indicators of tsunamis has been a matter of debate as boulder accumulations can also result from storm wave action. However, detailed studies (Noormets *et al.*, 2004; Nott, 2004; Scheffers *et al.*, 2005) have shown that extreme storm waves are not as efficient as tsunamis in the detachment and transport of large boulders. Noormets *et al.* (2004) indicated that tsunamis, as well as large

Fig. 7. Detailed photographs of the Akumal sector. (A) Reef cobbles and pebble ridge associated with Hurricane Emily in 2005. (B) Boulder ridge up to 5 m a.s.l. with attached (in the foreground of the picture) reef cobbles and pebbles associated with hurricane-generated waves recorded in the last decade. (C) Boulder ridge in the residential area north of Akumal. (D) Boulder ridge associated with a marine platform up to 70 m wide.

swell waves, are capable of quarrying large boulders, provided that sufficient initial fracturing is present. However, swell waves are seldom capable of emplacing large blocks onto the emerged platform due to their rapid disintegration after breaking. On the contrary, tsunamis are more likely to emplace large boulders onto the coastal platform due to the longer duration of their action. Mastronuzzi *et al.* (2007) identified the presence of rampart/ridge imbricated boulder accumulations along the coast of south-eastern Salento (Apulia region, Italy) associated with a historical tsunami.

Engel *et al.* (2013) in their paper on extreme wave deposits in Bonaire, southern Caribbean studied the size of boulders and sedimentary patterns of extreme wave deposits. These authors concluded that flooding events significantly exceeding the magnitude of recent category 5 hurricanes occurred in prehistoric times and that these flooding events were tsunamis.

Scheffers & Kinis (2014) described multiple imbricated boulder deposits (most of them as ramparts or ridges) with storm or tsunami origins. These authors completed a comprehensive review of existing literature and concluded that all of these imbricated boulder deposits were associated with tsunamis: Bishop & Hughes (1989) from coastal boulders in eastern Australia; Kelletat & Schellmann (2002) as well as Whelan & Kelletat (2002) from Cyprus; Bartel & Kelletat (2003) from Mallorca (Mediterranean Spain); Whelan & Kelletat (2003) as well as Kelletat *et al.* (2005) from Cabo Trafalgar and Mallorca (Spain); Gracia *et al.* (2006) also from Cabo Trafalgar in Andalusia, Spain; Kelletat *et al.*

Fig. 8. Detailed photographs of the Cozumel sector. (A) Angular to sub-angular cobble ridge up to 2·5 m a.s.l. (B) Large angular reef boulder at seaward edge of the ridge base associated with a fractured marine platform. Note the imbricated boulders behind the main boulder. (C) Boulder ridge up to 3 m a.s.l. associated with a marine platform. (D) Isolated reef boulder at the foot of the ridge.

(2004) from Eleuthera and Long Island, the Bahamas; Mastronuzzi & Sansò (2004) as well as Mastronuzzi *et al.* (2006) from several places in Apulia (south-eastern Italy); Scheffers (2006) from Cyprus, southern Turkey, Rhodes (Greece), and the Bahamas; Bryant & Haslett (2007) in tsunamites of the Bristol Channel in south-west England; Bryant (2008) from many places along the Australian shorelines; Scheffers *et al.* (2008a,b) in the western and southern Peloponnesos of Greece; Mhammdi *et al.* (2008) along the Moroccan coastline in the Rabat area; Maouche *et al.* (2009) in giant clasts along the Algerian coastline; Vött & May (2009) on the western and southern Peloponnesos, Greece; Hoffmann *et al.* (2010) in Oman; May *et al.* (2010) at Cape Bon in Tunisia; Scheffers *et al.* (2010) at many places along the Irish west coast; Vött *et al.* (2010) on Kephalonia island, Greece; Shah-hosseini *et al.* (2011) in southern Iran; and Vött *et al.* (2011) at the west coast of the Peloponnesus, Greece.

After reviewing multiple sets of data, Scheffers & Kinis (2014) concluded that generally, strong imbrication, even in large boulders (from 10 to >200 tons in weight), is best developed in coarse tsunami deposits. Also, these authors indicated that well-developed imbrication, in addition to the presence of balancing boulders perched delicately on top of boulder clusters or boulder ridges (although rare compared to overall imbrication), was indicative of tsunami impact, and excluded storm waves as the cause of these features.

Spiske & Bahlburg (2011) reviewed published examples of boulder transport by tsunamis (Goto

et al., 2007; Kelletat *et al.*, 2007; Paris *et al.*, 2009, 2010; Bourgeois & MacInnes, 2010; Lamarche *et al.*, 2010). This study concluded that various criteria, for example the size and mass of boulders, as well as the distance of the boulder deposits from the coast and their position above sea-level, were frequently used to discriminate between a tsunami or storm origin (Mastronuzzi & Sansò, 2000; Bryant & Nott, 2001; Whelan & Kelletat, 2005; Scheffers *et al.*, 2009) and that boulders entrained and transported by tsunamis were supposed to have larger sizes and greater mass, and should be transported further inland than storm boulders (Whelan & Kelletat, 2005; Scheffers *et al.*, 2008a, b; Goto *et al.*, 2009).

Other authors that assigned a tsunami origin to boulder ridges include Mhammdi *et al.* (2008) who described trains of large imbricated boulders along the Rabat coast (Morocco), possibly emplaced by the 1755 Lisbon tsunami. Costa *et al.* (2011) studied scattered boulders and boulder ridges in the Algarve (south Portugal) using the equations of Nott (Nott, 1997, 2003) and their modifications (Nandasena *et al.*, 2011a,b), correlating those deposits with the 1755 Lisbon earthquake tsunami. Medina *et al.* (2011) also described trains of imbricated boulders in Rabat and Larache (Atlantic Moroccan coast) and concluded that tsunami waves were responsible for the displacement of the largest boulders, whereas storm waves may have displaced smaller ones. Miller *et al.* (2014) studied coral boulder ridges in north Jamaica and concluded that they could have been derived by either storms or tsunamis. Roig-Munar *et al.* (2018) indicated a tsunami origin for large imbricated boulder ridges in Menorca (Balearic Island). Schneirder *et al.* (2018) surveyed large imbricated boulder trains along the north-eastern coast of Oman and related them with historical tsunamis associated with the Makran Subduction Zone.

Etienne *et al.* (2011) argued that there are no published accounts of extensive boulder ridge formations by tsunamis in any case studies of recent events. However, this statement can be challenged when looking at, for example, the 2004 Indian Ocean tsunami. Paris *et al.* (2009) and Nandasena *et al.* (2011b) have described boulder trains deposited by this tsunami in West Banda Aceh, Sumatra. Yamada *et al.* (2014) described concentrations of boulders (instead of ridges or alignments) in three major clusters, in relation to the 2011 Tohoku-oki tsunami at Miyako City, Japan. Recently Lau *et al.* (2018) identified lines of large coral reef boulders in Fiji, associated with a 1953 tsunami. The above findings by Etienne *et al.* (2011) are based on the concept that the organization of coarse clasts into ridges requires repeated reworking by many waves rather than by the impact of only a few waves, as occurs during a tsunami. This contradicts studies about the reworking of ridges by some researchers who found that if the different waves of a tsunami wave train had sufficient energy to entrain clasts, the transport would occur step by step in a landward direction (Spiske & Bahlburg, 2011). The process of entrainment, transport and deposition will be repeated two or three times, thus building the groups which then give the appearance of a single transport sequence. The proposed multi-step process model has been also reported in other tsunami boulder transport studies (Nandasena *et al.*, 2011b). As a result, the discussion about the origin of boulder ridges as a result of extreme wave events is still open and a range of approaches and interpretations exists in the literature.

MODELLING BOULDER TRANSPORT

Several studies have tried to infer the height of waves required to transport boulders at the coast, some of which have been previously cited in this text. Nott (1997, 2003) asserted that the pre-transport situation of a coastal boulder, relative to mean water level, along with its shape, size and density determines the height of wave required for it to be transported. Nott (2003) presented formulas used to calculate wave heights required to move boulders by both tsunami and storm waves in three different pre-transport situations: submerged boulders; subaerial boulders; and joint-bounded blocks. Noormets *et al.* (2004) noted that tsunami waves have a considerably longer wave period than storm waves, and thus may have greater transport capacity because each wave has the potential to move blocks for a longer time than a storm wave. Indeed, storm waves can break and emplace megaclasts but they tend to attenuate faster than tsunami waves. Pignatelli *et al.* (2009) introduced some modifications to the Nott (2003) formulas to incorporate the fact that a boulder has one side facing the wave, one top surface and is limited by four sides. Later, Barbano *et al.* (2010) modified their earlier proposal

after testing wave transport equations on the coast of Sicily. Nandasena *et al.* (2011a) improved the Nott equations further and found that the minimum flow velocity, derived from their revised equation, required to initiate transport of submerged boulders was less than that inferred from the Nott equations (for example, wave height required to move submerged boulders is reduced up to 56% and for joint bounded blocks up to 65%). These authors also developed a 'boulder transport histogram' to represent the range of flow velocities that satisfied the requirements for initial transport of a boulder via different modes of transport: sliding, rolling and saltation (Nandasena *et al.*, 2011a). The boulder transport histogram can be used to predict the possible initial transport modes of a boulder departing from the flow velocity.

Even inferring wave height from the 'initiation of motion' approach is currently considered questionable, although it has been used in previous work. Mastronuzzi *et al.* (2007) used the Nott (2003) equations for hydrodynamic calculations relating to boulder accumulations in south-eastern Salento (Italy). Additionally, other researchers used this methodology to study the movement of boulders related with extreme wave events, in studies by Spiske *et al.* (2008) in the Lesser Antilles (Caribbean), Maouche *et al.* (2009) on the Algeria coast, Switzer & Burston (2010) on the south-east Australian coast, Costa *et al.* (2011) on the Algarve (south Portugal) and Spiske & Bahlburg (2011), that applied this methodology to study the motion of cobbles and boulders during the 2011 Maule Tsunami (Chile). Engel & May (2012) and Engel *et al.* (2013) reviewed and applied the equations of Nandasena *et al.* (2011a) in Bonaire (Lesser Antilles, Caribbean) and their results indicated that boulder mass and dimensions, and thus the calculated wave energy and wave heights had been overestimated in most previous studies, demonstrating the importance of accurately calculating these parameters. Additionally, Spiske *et al.* (2008) reported that realistic bulk densities are critical for inferring minimum storm and tsunami wave heights from the boulder record.

Extreme wave height

Taking all of these formulas into account, and since most of the boulders examined in this study correspond to a JBB scenario, the equations below have been utilized. The Nott (2003) equation for joint-bounded boulders (JBB):

$$\mathrm{Ht} \geq \frac{0 \cdot 25\left(\frac{\rho b - \rho w}{\rho w}\right) a}{C_L} \quad (1)$$

$$\mathrm{Hs} \geq \frac{\left(\frac{\rho b - \rho w}{\rho w}\right) a}{C_L} \quad (2)$$

where Ht = tsunami wave height; Hs = storm wave height; C_L = coefficient of lift (0·178); a = A axis of boulder; ρw = density of seawater = 1·02 g ml^{-1}; ρb = boulder density. The bulk density of similar deposits was determined to be between 2·07 to 2·40 g cm^{-3} by Engel & May (2012) and in this study an average density of 2·27 g cm^{-3} was used.

The proposal of Engel & May (2012), which used a modification of the Nott equations forwarded by Nandasena *et al.* (2011a,b) for the JBB scenario, where:

$$\mathrm{Ht} = \frac{(\rho b - \rho w) \cdot V \cdot (\cos\theta + \mu \cdot \sin\theta)}{2 \cdot \rho w \cdot C_L \cdot a \cdot b \cdot q} \quad (3)$$

$$\mathrm{Hs} = \frac{(\rho b - \rho w) \cdot V \cdot (\cos\theta + \mu \cdot \sin\theta)}{0 \cdot 5 \cdot \rho w \cdot C_L \cdot a \cdot b \cdot q} \quad (4)$$

where V = *c*orrected boulder volume, q = *b*oulder area coefficient (0·73), b = B axis of boulder, μ = *c*oefficient of static friction (0·65) and θ = *b*ed slope angle of the pre-transport setting.

Table 1 presents results obtained for a number of boulders considered representative of the accumulations addressed herein in terms of weight, distance to the sea and emplacement altitude. The results obtained using the Engel & May (2012) solutions for JBB scenarios indicate that to move the heaviest and largest boulders, tsunami wave height would need to exceed 2·0 to 2·9 m (based on mass of the largest boulder found in different locations in the study area). The height of storm waves capable of moving those blocks should be at least 8·0 m and 11·5 m, respectively. Using the Nott (2003) formulas in the same scenario generally results in an underestimation of wave height in both the tsunami and storm wave cases.

Flow velocity and flow depth required to move the boulders

For the boulder transport histogram introduced by Nandasena *et al.* (2011a,b) and in the case of a submerged or subaerial boulder the following scenarios exist.

1 Transport initiates with sliding:

$$u^2 \geq \frac{2(\rho b/\rho w - 1)\mathrm{gc}(\mu_s cos\theta + \sin\theta)}{C_d(c/b) + \mu_s C_L} \quad (5)$$

2 Transport initiates with rolling (overturning):

$$u^2 \geq \frac{2(\rho b/\rho w - 1)\mathrm{gc}(cos\theta + (c/b)\sin\theta)}{C_d(c^2/b^2) + C_L} \quad (6)$$

3 Transport initiates with saltation:

$$u^2 \geq \frac{2(\rho b/\rho w - 1)\mathrm{gc}cos\theta}{C_L} \quad (7)$$

4 Or in the case of a joint-bounded block where transport begins with lifting:

$$u^2 \geq \frac{2(\rho b/\rho w - 1)\mathrm{gc}(cos\theta + \mu_s \sin\theta)}{C_L} \quad (8)$$

In Eqs 5 to 8, u is the flow velocity, g is gravitational acceleration (9·81 m s^{-2}), μ_s is the coefficient of static friction between the boulder and the bed (0·7), and C_d is the coefficient of drag (1·95) (Nandasena *et al.*, 2011a,b; Nandasena *et al.*, 2014).

To estimate the flow departing depth from the minimum flow velocity required to move a boulder, Nandasena *et al.* (2014) proposed a relationship between flow depth and flow velocity described by the Froude number as $\mathrm{Fr} = u/\sqrt{\mathrm{gh}}$, where h is the flow depth. The Froude number for past tsunamis has been determined to be between 0·7 and 2·0; in this study values of 1·0 and 1·5 were used, as proposed by Nandasena *et al.* (2012, 2014).

The results obtained by applying these formulas to boulders examined in this study (considering weight, distance to the sea or altitude) are presented in Table 2 and Fig. 9 shows the corresponding boulder transport histogram. Table 2 and Fig. 9 also display the minimum flow velocity and range of flow velocities required to initiate boulder transport at each site. The average results indicate that a wave celerity of not less than 3·0 m s^{-1} would have been required to transport boulders from their pre-transport location. If the average flow velocity was >3·0 m s^{-1}, the boulders would have been transported by sliding. If the average flow velocity is >4·3 m s^{-1}, the boulders would have been transported by rolling; if average flow velocity is >9·1 m s^{-1}, boulder transport would have been via saltation. For JBBs, the average flow velocity for transport by lifting is >9·3 m s^{-1}.

Table 2 also indicates the flow depths necessary to initiate boulder transport using the formulas applied here. Nandasena *et al.* (2014) indicated the difficulty in establishing the Froude number at each site. Using Fr = 1·0, the minimum flow depth necessary to allow for: (i) sliding ranges from 0·4 to 2·1 m (average 1·0 m); (ii) rolling ranges from 0·6 to 5·3 m (average 2·1 m); and (iii) for saltation ranges from 2·6 to 16·5 m (average 8·8 m). Lifting, as is the case of JBB, required flow depths between 2·7 m and 17·1 m (average 9·1 m). When using Fr = 1·5 the minimum flow depth for: (i) sliding changes to 0·2 to 0·9 m (average 0·4 m); (ii) rolling changes to 0·2 to 2·3 m (average 0·9 m); and (iii) saltation changes to 1·2 to 7·3 m (average 3·9 m). Initiation by lifting requires that the minimum flow depth ranged between 1·2 m and 7·6 m (average 4·0 m), a value more applicable to the boulder ridges recorded in this study.

TSUNAMI VERSUS HURRICANE ORIGIN

Seismicity in the Yucatán Peninsula

The Yucatán Peninsula is considered to be a tectonically stable area at least in the period since the late Pleistocene (Szabo *et al.*, 1978). The Mexican Seismic Service (SSN, 2018) has only registered four earthquakes in the Yucatán Peninsula since 1990, and all with a Mw lower than 4·6. Tsunami catalogues in the Caribbean area show no recorded events for the Quintana Roo coast (compiled in Engel *et al.*, 2016). The tsunamigenic earthquakes in the Caribbean Plate are mostly concentrated along the western (Lesser Antilles), north-western (Muertos Thrust Belt)

Table 2. Minimum values of flow velocity and flow depth required to initiate boulder transport in different transport modes and using different Froude numbers (F_r = 1; F_r = 1·5).

	Minimum flow velocity required to initiate boulder transport (m s^{-1})				Minimum flow depth necessary to initiate boulder transport (m)							
					F_r = 1·0				F_r = 1·5			
Boulder ID	Sliding	Rolling	Saltation	Lifting	Slid.	Roll.	Saltat.	Lift.	Slid.	Roll.	Saltat.	Lift.
BPM1	3·3	5·3	8·3	8·4	1·1	2·9	7·0	7·3	0·5	1·3	3·1	3·2
BPM2	2·0	2·3	7·9	8·0	0·4	0·6	6·3	6·6	0·2	0·2	2·8	2·9
BPM3	2·6	3·8	7·8	7·9	0·7	1·5	6·2	6·4	0·3	0·6	2·8	2·9
BPM5	2·6	3·2	9·7	9·9	0·7	1·1	9·6	10·0	0·3	0·5	4·3	4·4
BPM6	3·1	4·3	10·0	10·2	1·0	1·9	10·2	10·5	0·4	0·8	4·5	4·7
BPM7	2·6	3·7	8·1	8·3	0·7	1·4	6·7	7·0	0·3	0·6	3·0	3·1
BPM8	2·9	4·1	8·6	8·8	0·8	1·7	7·6	7·8	0·4	0·8	3·4	3·5
BPM9	4·6	7·2	12·0	12·2	2·1	5·3	14·7	15·3	0·9	2·3	6·5	6·8
BPM10	3·7	5·7	10·4	10·6	1·4	3·3	11·0	11·4	0·6	1·5	4·9	5·1
B2-3	3·0	4·3	9·3	9·5	0·9	1·9	8·8	9·1	0·4	0·8	3·9	4·1
B2-4	2·6	3·5	8·5	8·6	0·7	1·2	7·3	7·6	0·3	0·5	3·2	3·4
B2-5	2·8	3·8	8·8	9·0	0·8	1·5	8·0	8·3	0·3	0·7	3·5	3·7
BPM11	2·5	3·3	8·8	8·9	0·6	1·1	7·8	8·1	0·3	0·5	3·5	3·6
BPA1	2·8	3·3	10·8	11·0	0·8	1·1	12·0	12·4	0·4	0·5	5·3	5·5
BPA2	3·3	4·4	11·3	11·5	1·1	2·0	13·1	13·5	0·5	0·9	5·8	6·0
BPA3	2·8	3·6	10·2	10·4	0·8	1·3	10·6	11·0	0·4	0·6	4·7	4·9
BPA4	2·8	4·0	8·8	8·9	0·8	1·6	7·8	8·1	0·4	0·7	3·5	3·6
BPA5	2·8	3·3	11·0	11·2	0·8	1·1	12·2	12·7	0·4	0·5	5·4	5·6
BPA7	2·2	2·7	8·2	8·4	0·5	0·7	6·9	7·1	0·2	0·3	3·1	3·2
BPA8	3·4	5·4	8·8	8·9	1·2	3·0	7·8	8·1	0·5	1·3	3·5	3·6
BPA9	3·0	3·4	11·6	11·8	0·9	1·2	13·8	14·3	0·4	0·5	6·1	6·3
BPA10	3·7	5·1	12·1	12·3	1·4	2·7	14·9	15·4	0·6	1·2	6·6	6·8
BPA11	3·3	4·8	9·8	10·0	1·1	2·4	9·8	10·1	0·5	1·0	4·3	4·5
BKAN1	2·7	3·4	10·1	10·3	0·8	1·1	10·5	10·8	0·3	0·5	4·6	4·8
BKAN2	2·7	4·0	8·0	8·1	0·8	1·7	6·5	6·7	0·3	0·7	2·9	3·0
BKAN3	2·7	4·3	6·6	6·7	0·7	1·9	4·4	4·6	0·3	0·8	2·0	2·0
BKAN4	4·0	6·4	9·7	9·9	1·6	4·2	9·6	10·0	0·7	1·9	4·3	4·4
BKAN5	3·2	5·1	8·4	8·5	1·1	2·7	7·2	7·4	0·5	1·2	3·2	3·3
BKAN6	2·7	4·4	5·2	5·3	0·7	2·0	2·8	2·9	0·3	0·9	1·2	1·3
BKAN7	3·2	5·4	7·2	7·3	1·1	3·0	5·2	5·4	0·5	1·3	2·3	2·4
BKAN8	2·5	3·8	7·4	7·6	0·7	1·4	5·6	5·8	0·3	0·6	2·5	2·6
BKAN9	3·9	6·5	8·3	8·4	1·6	4·3	7·0	7·3	0·7	1·9	3·1	3·2
BKAN10	3·6	5·0	11·6	11·8	1·3	2·6	13·8	14·3	0·6	1·1	6·1	6·3
BXC4	2·3	2·7	8·7	8·8	0·5	0·8	7·7	8·0	0·2	0·3	3·4	3·5
B2	2·4	2·8	9·1	9·2	0·6	0·8	8·4	8·7	0·3	0·4	3·7	3·9
B6	2·8	3·6	10·2	10·4	0·8	1·3	10·6	11·0	0·4	0·6	4·7	4·9
BA12	2·9	3·7	10·6	10·8	0·9	1·4	11·6	12·0	0·4	0·6	5·1	5·3
BN1	2·9	3·8	10·1	10·2	0·9	1·5	10·3	10·7	0·4	0·7	4·6	4·8
BN3	2·2	3·0	7·3	7·5	0·5	0·9	5·5	5·7	0·2	0·4	2·4	2·5
BN5	3·1	4·3	10·1	10·3	1·0	1·9	10·5	10·8	0·4	0·9	4·6	4·8
BN6	3·1	5·0	7·5	7·7	1·0	2·5	5·8	6·0	0·4	1·1	2·6	2·7
BAK2	3·2	5·2	8·1	8·3	1·1	2·7	6·7	7·0	0·5	1·2	3·0	3·1
BAK3	2·9	3·7	10·6	10·8	0·9	1·4	11·6	12·0	0·4	0·6	5·1	5·3
BAK4	2·9	3·6	10·8	11·0	0·9	1·3	12·0	12·4	0·4	0·6	5·3	5·5
BAK5	3·1	5·1	7·2	7·3	1·0	2·6	5·2	5·4	0·4	1·2	2·3	2·4
BAK6	3·0	3·7	10·8	11·0	0·9	1·4	11·8	12·3	0·4	0·6	5·3	5·4
BCZ3	2·8	4·5	5·1	5·2	0·8	2·1	2·6	2·7	0·4	0·9	1·2	1·2
BCZ4	3·0	4·9	6·6	6·7	0·9	2·5	4·4	4·6	0·4	1·1	2·0	2·0
BCZ5	2·8	4·2	8·3	8·4	0·8	1·8	7·0	7·3	0·4	0·8	3·1	3·2
BCZ6	4·3	7·0	10·5	10·7	1·9	5·0	11·3	11·7	0·8	2·2	5·0	5·2
BCZ7	3·7	4·8	12·7	13·0	1·4	2·4	16·5	17·1	0·6	1·1	7·3	7·6
BCZ8	3·5	5·7	6·4	6·5	1·3	3·3	4·1	4·3	0·6	1·5	1·8	1·9
BCZ9	4·0	6·4	9·7	9·9	1·6	4·2	9·6	10·0	0·7	1·9	4·3	4·4

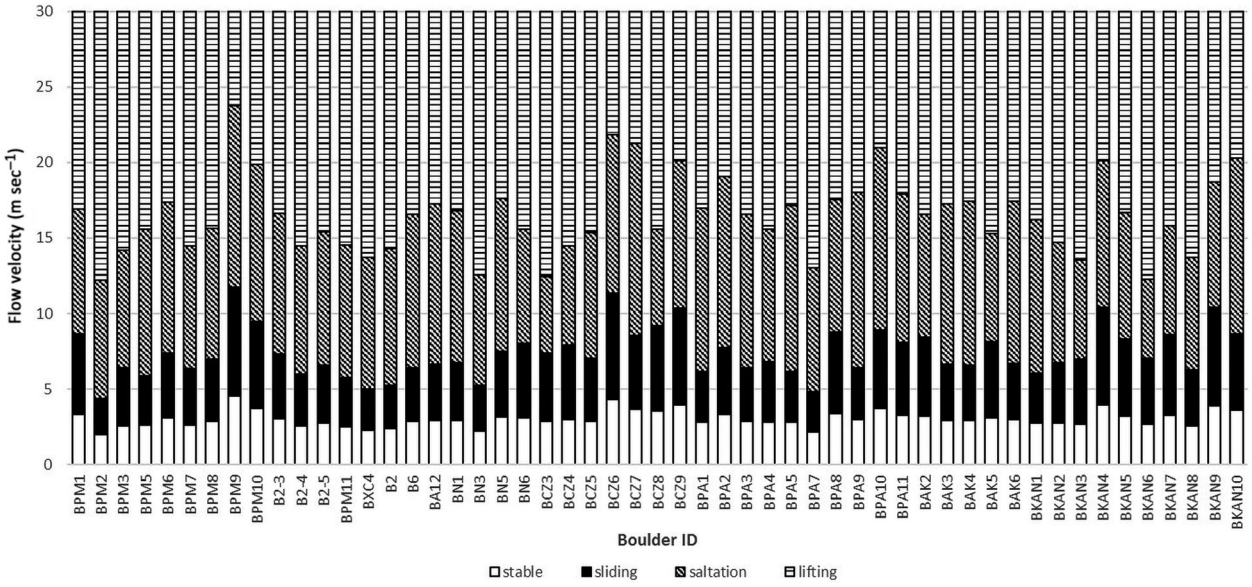

Fig. 9. Boulder transport histogram for the boulders recorded at the study sites (see Tables 1 and 2 for boulder properties and pre-transport settings).

and south-western (South Caribbean Deformed Belt) plate boundaries (USGS, 2018). In addition, models of tsunami propagation (Engel *et al.*, 2016) show that a tsunami generated by a Mw 7·9 earthquake from the Muertos Thrust Belt (MTB) cannot reach the Yucatán coast. A tsunami triggered by a Mw 8·8 earthquake from the South Caribbean Deformed Belt (SCBD) would reach the north-eastern Yucatán coast with a wave height <1·0 m, thus not high enough to have produced the boulder ridges investigated in this study.

Therefore, an alternative source of seismic activity is required to generate a tsunami wave able to reach the eastern coast of Yucatán and confirm a tsunami origin for the boulder ridges. Two recent earthquake events off the coast of Honduras (Mw 7·3, 2009 and Mw 7·6, 2018; USGS, 2018) and a third one in Guatemala (Mw 7·5, 1976; USGS, 2018) associated with the Motagua/Swan Island Fault System (MSFS), identify this region as a possible source for tsunamigenic earthquakes. Likewise, two late Holocene Mw > 7 earthquakes, have been reported by Cox *et al.* (2008) pre-dating the 2009 and 2018 events, leading these authors to propose a 1000-year recurrence interval for large earthquakes (Mw > 7) associated with the MSFS.

The MSFS is a left-lateral strike-slip fault, segment of the boundary between the North American and Caribbean plates, which accommodates approximately 20 mm year^{-1} slip (USGS, 2018). However, the instrumental and palaeoseismic earthquake records presented above indicate that, despite the relatively low slip rate of the MSFS, the resulting seismic and tsunami potential can be significant.

Hurricanes in the Yucatán Peninsula

Hurricanes commonly occur in this region, with the Yucatán Peninsula exposed to an average of 20 tropical cyclones over a 150 year period (Rosengaus Moshinsky *et al.*, 2014). In order to characterize the extreme wave climate and storm surges in the Mexican Pacific Ocean and Gulf of Mexico/Caribbean Sea, Meza-Padilla *et al.* (2015) modelled a total of 3100 synthetic events achieving landfall in Mexico. These events were divided between both basins and it was found that the highest waves are expected in the Mexican Caribbean and the northern coast of the Gulf of Mexico, whilst the highest storm surge occurred in the northern part of the Yucatán Peninsula. Some of the most destructive hurricanes to have made landfall in the eastern Yucatán produced waves with heights of 4 m and, in the case of Hurricane Gilbert (1988), inundated up to 5 km inland. Hurricane Gilbert; the strongest hurricane that has reached the Mexico coast achieved a category 5 on the Saffir-Simpson scale, advancing almost 85 km

inland (Rosengaus Moshinsky & Sánchez Sesma, 1990). Other destructive hurricanes include: Hurricane Emily in 2005 (López López, 2011) where 3 m high waves from a combined tide and surge resulted in a 4 m sea-level rise; and Hurricane Wilma also in 2005 (Alva González, 2015) with its 8 m storm tide. These wave heights were measured by buoys located at some considerable distance from the coast (260 km) and so are likely to have reached the coast at heights of <4 m due to dissipation of wave energy (Guisado-Pintado *et al.*, 2014). Coastal waves of even 4 m would still have been too small to have produced the ridges recorded in this study. Eyewitness reports in the Chemuyil area, where the most extensive accumulations of reef cobbles and pebbles were recorded, indicated that most of them were deposited during Hurricane Emily and were later reworked by Hurricane Wilma. Eyewitnesses also reported that the pre-existing boulders forming the main ridge were not moved in either hurricane event.

On the nearby coast of Belize, McCloskey & Liu (2013) described extreme wave events related to increases in tropical cyclone activity by recording the input of detrital sediments in some environments. These authors concluded that the activity pattern recorded in their study did not match the regional records from either the northern Gulf of Mexico or the north-eastern Caribbean/Atlantic coast and supported the idea that hurricane activity regimes are not synchronous across the North Atlantic, with different regions displaying different temporal patterns. Also in Belize, Denommee *et al.* (2014) presented sedimentary proxy data for palaeohurricane activity from two sediment cores and related this activity to washover deposits characterized by an increase in grain size. These authors proposed a seismic origin for these deposits, concluding that: "unfortunately, there are no widely applicable diagnostic criteria to distinguish storm versus tsunami-generated event beds in such a depositional setting" (Denommee *et al.*, 2014).

The record of hurricanes is also controversial in any coastal karstic environment. Brown *et al.* (2014) studied Laguna Chumkopó, in a coastal karst basin in the eastern coast of Yucatán Peninsula, and showed that only one of the three last intense events [Hurricanes Gilbert (1988), Emily (2005) and Wilma (2005)] was recorded in the sediment (Gilbert 1988) as a fining-upward sequence.

Modelling a tsunami in the eastern Yucatán Peninsula

The tectonic stability of the Yucatán Peninsula region has been used as an argument to disprove the occurrence of tsunamis in this area even during historical times. It is proposed here that seismicity associated with the Motagua/Swan Island Fault System (MSFS) could originate a tsunami in this Caribbean area. To test this hypothesis a model of a tsunami generated by a seismic event located in the MSFS has been generated simulating a Mw 7·6, earthquake at 19 km depth with a 110 km long and 26 km wide rupture area. These parameters were based on recent events off the coast of Honduras (Mw 7·3, 2009 and Mw 7·6, 2018; USGS, 2018) and a third one in Guatemala (Mw 7·5, 1976; USGS, 2018) associated with the MSFS. The fault is type node plane 2 (NP2), with a left lateral strike-slip focal mechanism, coherent with the regional tectonic setting. Similar parameters have been calculated in other left-lateral strike-slip faults (Rizza *et al.*, 2011). The numerical code used in this study was Tsunami-HySEA, a GPU-based shallow water code, developed by the EDANYA Group (University of Málaga) and extensively benchmarked for tsunami simulations (Macías *et al.*, 2017). For the numerical simulation, a two-way nested mesh technique (as in Macías *et al.*, 2016) was used. The global mesh that covers the computational domain has a resolution of 15 arc sec (*ca* 450 m). Six nested meshes, with an enhanced resolution of 0·9375 arc sec (*ca* 28 m) are used in the coastal strip to improve the morphological resolution of the sea floor and thus the spatial distribution of tsunami wave height. Results at ×32 resolution show that a wave height of *ca* 2·0 m would be generated in the studied area (Fig. 10). Applying the proposed intensity scale of tsunami environmental effects (TEE-16 Scale; Lario *et al.*, 2016), the tsunami intensity observed in the study area would be VI to VII (slightly damaging to damaging) but this does not represent the maximum intensity because the area is at a considerable distance from the source.

DISCUSSION

Origin of the boulder ridges

Using different approaches, observations in the current study demonstrated that in order to

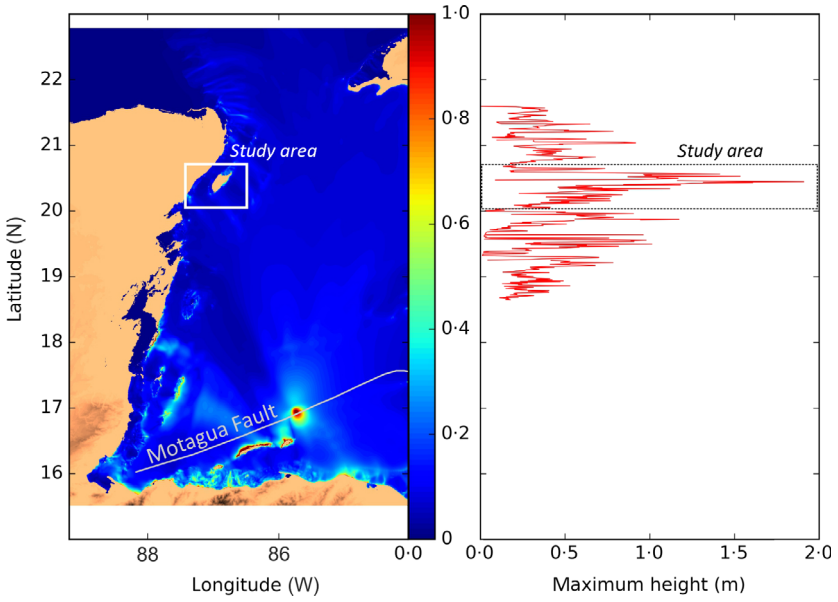

Fig. 10. Model of a tsunami generated by a Mw 7·6 earthquake along MSFS showing spatial distribution of predicted maximum wave height. Left panel shows the whole computational domain (colour scale in metres saturated to 1 m) and the right panel shows maximum wave height near to the coast in the studied area.

move the heaviest and largest boulders present in the described ridges, storm waves must have attained heights of between 8·0 m and 11·5 m. As described previously, there are no historical data of waves of this magnitude during recent and intense hurricanes affecting the area. Data show that during the last century (1900 to 2002) 12 tropical storms and 46 hurricanes reached the Yucatán Peninsula (UNYSIS Data Base from Hurricanes; http://weather.unisys.com/hurricanes). In addition, from 1851 to 2011 in Quintana Roo, seven hurricanes (scale 4 and 5) reached the coast (Ihl & Frausto, 2014), without any evidence of boulder transportation. In support of this, the only geological evidence for hurricane clast transport (supported by eyewitnesses) consists of movements of reef cobbles and pebbles that were able to overpass the boulder ridge (such as in Chemuyil) or became attached to the seaward side of the boulder ridges. If 20th Century category 5 hurricanes have not been able to move reef boulders, it seems plausible to assign a tsunami origin to the extreme wave event that resulted in the formation of the boulder ridges studied. Medina-Elizalde *et al.* (2016) used other proxy data (δ^{18}O-derived precipitation levels recorded from a stalagmite in the Yucatán Peninsula) and found that regional palaeo-storm records suggested that tropical storm activity in the Yucatán Peninsula was either similar to or significantly lower than today during the TCP (Terminal Classic Period; AD 750–950). Therefore, perhaps some of the 'washover' events identified in the literature of similar age may not have been caused by hurricane events.

Furthermore, the height of a tsunami wave required to move the heaviest and largest boulders studied in these ridges would need to have been between 2·0 m and 2·9 m. This height is compatible with wave heights simulated by the numerical model developed in this study. Therefore, it is reasonable to propose a tsunami generated by an earthquake (Mw > 7·6 offshore in the eastern Caribbean sector of the MSFS) as the extreme wave event that resulted in the formation of the main ridge in this study. The smaller ridge overlapping the main boulder ridge was generated by Hurricane Wilma in 2005 (based on interviews from witnesses), demonstrating that destructive hurricanes do not have sufficient energy in this area to generate the larger boulder ridges. Some authors have even suggested that coral boulder ridges and single coral boulders may have a complex, long-term history of transport, accumulation and modification produced by multiple and intensive storms (Morton *et al.*, 2008; Etienne *et al.*, 2011; Scheffers *et al.*, 2014; Rixhon *et al.*, 2018). Others propose a multi-step process during a tsunami, where the process of entrainment, transport and deposition is repeated two to three times, thus building the groups but may be interpreted as a single transport sequence (Nandasena *et al.*, 2011b; Spiske & Bahlburg, 2011).

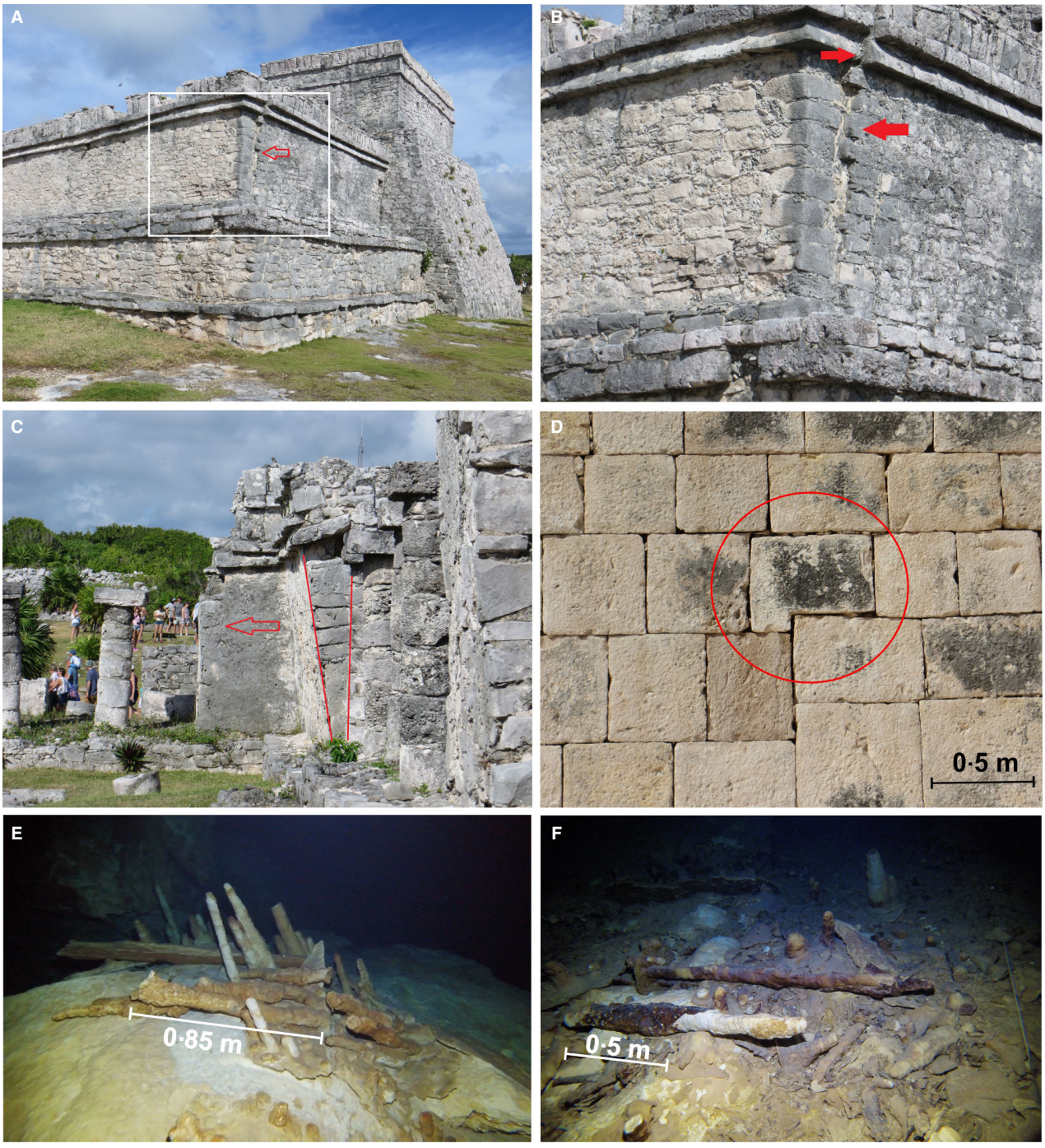

Fig. 11. Evidence of palaeoseismicity in the Yucatán Peninsula. (A) to (C) Correspond to archaeoseismological features described by Rodríguez-Pascua *et al.* (2011) as primary effects that occur when the ground transmits seismic waves to buildings. (A) and (B) Displaced walls at the Tulum archaeological site (main building height 12 m). (C) Tilted walls in a structure at the Tulum archaeological site (column height 1·90 m); tilting occurs as a consequence of horizontal ground movement which affects the wall foundations. (D) Reconstruction techniques as the result of previous seismic activity producing intense ground shaking. This reconstruction is observed at Chichen Itza archaeological site. In this case it consists of interlocked blocks, usually used as a reconstruction technique after seismic damage, as has been observed in other areas of Mexico (Giner-Robles *et al.*, 2012). (E) and (F) Effects of palaeoseismicity present in submerged cave systems from Quintana Roo. (E) Tilted, collapses and orientated speleothems in the Tajma Ha cenote. (F) Collapses and orientated speleothems in the Minotauro cenote.

Tsunami age and palaeoseismic implications

Dating of wave-emplaced blocks and boulders is still a challenge (Terry *et al.*, 2013; Engel *et al.*, 2016; Rixhon *et al.*, 2018). The main boulder ridges seem to be associated with a single large extreme wave event. However, it is challenging to provide a definitive date for boulder emplacement in the ridges without the presence of *Lithophaga* sp. shells or other boring organisms within the boulders, assuming that they were living just prior to boulder removal from their natural habitat. Shaw & Benson (2015) recorded and dated peat deposits beneath the boulder ridge in the Akumal area, thus pre-dating the emplacement of the main boulder ridge. Carbon-14 dating of the peat provided 2σ calibrated ages for two samples (1390 to 1567 and 1348 to 1613 cal yr BP), which are compatible with a tsunami event dated to *ca* 500 to 800 AD, during the late Classic period. In some locations within the region, it is possible to observe Mayan buildings constructed on top of, and therefore post-dating, the boulder ridges. Examples can be found in the Xcaret complex (Fig. 3) or at Punta Chile (north Kantenah–south-west Xpu Ha; Fig. 6). Despite the different phases of construction, these remains are 'Costa oriental' (Eastern coast) in style, meaning Post-Classic Mayan period, between 900 to 1521 AD (Andrews & Andrews, 1975; Zúñiga, 2016). This corroborates the inferred date of the tsunami event as being between 500 to 900 AD. It is remarkable that there is no evidence of settlements prior to the Post-Classic period in this coastal area, and it may be that any small settlements that did exist were affected by and covered by the tsunami deposits. This is also supported by Cox *et al.* (2008) who found evidence of a large Mw > 7·0 earthquake triggered in the MSFS in 900 AD, in uplifted coral reef platforms. This event would have affected at least the north coast of Honduras.

Regarding the possible storm origin of the boulder ridges, the total absence of boulders on top of the aforementioned Mayan remains is noteworthy, especially when taking into consideration that during the last century (1900 to 2002) almost 12 tropical storms and 46 hurricanes reached the Yucatán Peninsula (UNYSIS Data Base from Hurricanes; http://weather.unisys.com/hurricanes). In Belize, McCloskey & Liu (2013) found traces of an extreme erosional event post *ca* 2000 yr cal BP in sediments, which those authors described as: "a transition layer that contains sand and marine macrofossils, including a large shell, indicating a seaward point of origin for this large event, the most likely candidate is an intense hurricane". At a similar age in the stratigraphic record that is coherent with coseismic uplift "a sudden transition from deep water to shallow wetlands" was found. The authors hypothesized that a tsunami could be a possible cause of these deposits, but eventually discarded this hypothesis because this area is assumed as being 'tectonically stable'.

Confirmation of a likely tsunami event caused by a Mw > 7·6 earthquake on MSFS implies that even if a long recurrence interval exists, destructive tsunami episodes can reach the eastern Yucatán coast. Despite the belief that the area has been tectonically stable since the late Pleistocene this study presents additional evidence of seismic activity during Mayan times. The main evidence corresponds to archeoseismological features, similar to those described in other Mexican archaeological remains or elsewhere (Giner-Robles *et al.*, 2011, 2012; Rodríguez-Pascua *et al.*, 2011) and located in Mayan sites (for example, tilted walls, 'antiseismic' fabric, etc.). Other evidence of seismic events (Fig. 11) has been found in submerged cave systems (tilted speleothems, collapses and orientated speleothems, etc.) as well as faults affecting the late Pleistocene and Holocene reef deposits (eastern Cozumel), that are still being investigated (Lario *et al.*, 2017).

CONCLUSIONS

A semi-continuous boulder ridge standing up to 5 m above sea-level has been recorded on the eastern coast of the Yucatán Peninsula and Cozumel Island, generated by an extreme wave event. The application of different approaches demonstrated that waves of between 2·0 to 2·9 m (in the case of a tsunami origin) and between 8·0 to 11·5 m (in the case of storm/hurricane origin) would be required to produce dislodgement, transport and accumulation of the boulders in these ridges. All of the tropical storms and hurricanes recorded during the last 100 years have not generated waves that reached the coast with a wave height >4 m and there is no evidence of boulder transport during these events. Most of the possible tsunami source areas located in the eastern Caribbean are not capable of generating a tsunami that would reach the Yucatán coast. However, as demonstrated through model simulation in this study,

the Motagua/Swan Island Fault System section located in the south-west Caribbean basin can generate a tsunami with waves of between 2·0 to 3·0 m height at the eastern Yucatán coast, resulting from a Mw > 7·6 earthquake. Therefore, a tsunami origin seems the most reliable option to generate the extreme wave event that deposited the boulder ridge present in some sectors of the western Quintana Roo coastline. This, and other evidence presented here, demonstrates the occurrence of seismic activity during late Pleistocene and Holocene in the Eastern Yucatán Peninsula and surrounding areas illustrating the necessity to review all mitigation protocols in this area related to seismic and tsunami hazards.

ACKNOWLEDGEMENTS

Financial support by Spanish government projects CGL2013-42847-R and CGL2015-69919-R and SIMURISK (MTM2015-70490-C2-1-R). The GPU and multi-GPU computations have been performed at the Unit of Numerical Methods (UNM) of the Research Support Central Services (SCAI) of the University of Malaga. It is a contribution to the GTE IGCP Project 639 'Sea Level Change from Minutes to Millennia'. We appreciate the suggestions to improve the paper provided by reviewers Ricardo Ramalho, Max Engel and Associate Editor César Andrade.

REFERENCES

Agisoft (2017) *Agisoft PhotoScan User Manual.* Professional Edition, Version 1.3. Agisoft, San Petersburgo.

Alva González, O.J. (2015) *Evaluación de daños en la infraestructura de los estados de Quintana Roo y Yucatán causados por el huracán Wilma de 2005*. Tesis de Licenciatura. Facultad de Ingeniería, UNAM, Mexico, 84 pp.

Andrews, E.W. and **Andrews, A.P.** (1975) *A Preliminary Study of the Ruins of Xcaret, Mexico, with Notes on Other Archaeological Remains on the Central East Coast of the Yucatán Peninsula.* Middle American Research Institute, Publication 40, Tulane University, New Orleans, LA, 117 pp.

Barbano, M.S. Pirrota, C. and **Gerardi, F.** (2010) Large boulders along the south-eastern Ionian coast of Sicily: storm or tsunami deposits? *Mar. Geol.*, **275**, 140–154.

Bartel, P. and **Kelletat, D.** (2003) Erster Nachweis holozäner Tsunamis im Westlichen Mittelmeergebiet (Mallorca, Spanien) mit einem Vergleich von Tsunamiund Sturmwellenwirkung auf Festgesteinsküsten. *Ber. Forsch.* Technol.-Center, Kiel Busum **28**, 93–107.

Bishop, P.M. and **Hughes, M.G.** (1989) Imbricate and fitted fabrics in coastal boulder deposits on the Australian east coast. *J. Geol.*, **17**, 544–547.

Blanchon, P. Eisenhauer, A. Fietzke, J. and **Liebetrau, V.** (2009) Rapid sea-level rise and reef back-stepping at the close of the last interglacial highstand. *Nature*, **458**, 881–855.

Bourgeois, J. and **MacInnes, B.T.** (2010) Tsunami boulder transport and other dramatic effects of the 15 November 2006 central Kuril Islands tsunami on the island of Matua. *Z. Geomorphol.*, **54**, 175–190.

Brown, A.L., **Reinhardt, E.G.**, **van Hengstum, P.J.** and **Pilarczyk, J.E.** (2014) A coastal Yucatán sinkhole records intense hurricane events. *J. Coastal Res.*, **30**, 418–428.

Bryant, E. (2008) *Tsunami: The Underrated Hazard*. 2nd edn. Springer-Verlag, Berlin, 330 pp.

Bryant, E.A. and **Haslett, S.K.** (2007) Catastrophic wave erosion, Bristol Channel, United Kingdom: impact of tsunami? *J. Geol.*, **115**, 253–269.

Bryant, E.A. and **Nott, J.** (2001) Geological indicators of large tsunami in Australia. *Nat. Hazards*, **24**, 231–249.

Con, M.J. (1991) Trabajos recientes en Xcaret, Quintana Roo. *Estudios de Cultura Maya*, **18**, 65–129.

Costa, P.J.M., **Andrade, C.**, **Freitas, M.C.**, **Oliveira, M.A.**, **da Silva, C.M.**, **Omira, R.**, **Taborda, R.**, **Baptista, M.A.** and **Dawson, A.G.** (2011) Boulder deposition during major tsunami events. *Earth Surf. Proc. Land.*, **36**, 2054–2068.

Cox, R., **Lumsden, D.**, **Gough, K.**, **Lloyd, R.** and **Talnagi, J.** (2008) Investigation of late Quaternary fault block uplift along the Motagua/Swan Islands fault system: Implications for seismic/tsunami hazard for the Bay of Honduras. *Tectonophysics*, **457**, 30–41.

Denommee, K.C., **Bentley, S.J.** and **Droxler, A.W.** (2014) Climatic controls on hurricane patterns: a 1200-y near-annual record from Lighthouse Reef. *Belize. Sci. Rep.*, **4**, 1–7.

Engel, M. and **May, S.M.** (2012) Bonaire's boulder fields revisited: evidence for Holocene tsunami impact on the Leeward Antilles. *Quatern. Sci. Rev.*, **54**, 126–141.

Engel, M., **May, M.**, **Frenzel, P.**, **Scheffers, A.M.**, **Kelletat, D.** and **Brückner, H.** (2013) Holocene tsunamis in the southern Caribbean: Evidence from stratigraphic archives and the coarse-clast record. In: *Seismic hazard, critical facilities and slow active faults* (Eds C. Grützner, A. Rudersdorf, R. Pérez-López and K. Reicherter). Proceedings of the 4th International INQUA meeting on Paleoseismology, Active Tectonics and Archeoseismology (PATA Days), 9–15 October 2013, Aachen, Germany, 55–58.

Engel, M., **Oetjen, J.**, **May, S.M.** and **Brückner, H.** (2016) Tsunami deposits of the Caribbean – Towards an improved coastal hazard assessment. *Earth Sci. Rev.*, **163**, 260–296.

Etienne, S., **Buckley, M.**, **Paris, R.**, **Nandasena, A.K.**, **Clark, K.**, **Strotz, L.**, **Chagué-Goff, C.**, **Goff, J.** and **Richmond, B.** (2011) The use of boulders for characterising past tsunami: lessons from the 2004 Indian Ocean and 2009 South Pacific tsunami. *Earth Sci. Rev.*, **107**, 76–90.

Giner-Robles, J.L., **Silva, P.G.**, **Pérez-López, R.**, **Rodríguez-Pascua, M.A.**, **Bardají, T.**, **Garduño- Monroy, V.H.** and **Lario, J.** (2011) *Evaluación del daño sísmico en edificios históricos y yacimientos arqueológicos. Aplicación al estudio del riesgo sísmico*. Proyecto EDASI. Serie Investigación, Fundación MAPFRE, Madrid, 96 pp.

Giner-Robles, J.L., **Bardají Azcárate, T.**, **Rodríguez-Pascua, M.A.**, **Pérez-López Raúl Silva, P.G.**, **Garduño Monroy, V.H.** and **Lario, J.** (2012) Postseismic earthquake archaeological effects (EAE) in Morelia and Patzcuaro

cities (Michoacan, Mexico). In: *Proceedings 3 INQUA-IGCP 567 International Workshop on Active Tectonics, Paleoseismology and Archaeoseismology* (Eds V.H. Garduño and M.A. Rodríguez-Pascua), Morelia, Mexico, 254–258.

Goto, K., **Chavanich, S.A.**, **Imamura, F.**, **Kunthasap, P.**, **Matsui, T.**, **Minoura, K.**, **Sugawara, D.** and **Yanagisawa, H.** (2007) Distribution, origin and transport process of boulders deposited by the 2004 Indian Ocean tsunami at Pakarang Cape, Thailand. *Sed. Geol.*, **202**, 821–837.

Goto, K., **Okada, K.** and **Imamura, F.** (2009) Characteristics and hydrodynamics of boulders transported by storm waves at Kudaka Island, Japan. *Mar. Geol.*, **262**, 14–24.

Gracia, F.J., **Alonso, C.**, **Benavente, J.**, **Anfuso, G.** and **Del-Rio, L.** (2006) The different records of the 1755 tsunami waves along the south Atlantic Spanish Coast. *Z. Geomorphol.*, **146**, 195–220.

Guisado-Pintado, E., **Malvárez, G.**, **Navas, F.** and **Carrero, R.** (2014) Spatial distribution of storm wave energy dissipation for the assessment of beach morphodynamics. *J. Coastal Res.*, **70**, 260–265.

Hoffmann, G., **Reicherter, K.**, **Wiatr, T.**, **Grützner, C.** and **Rausch, T.** (2010) Boulder accumulations along the coastline between Fins and Sur (Sultanate of Oman) - tsunamigenic remains? *Nat. Hazards*, **65**, 851–873.

Ihl, T. and **Frausto, O.** (2014) El cambio climático y los huracanes de la península de Yucatán. In: *Monitoreo de riesgo y desastre asociado a fenómenos hidrometeorológicos extremos y cambio climático* (Ed. O. Frausto), pp. 20–30. Universidad de Quintana Roo, Quintana Roo.

Kelletat, D. and **Schellmann, G.** (2002) Tsunamis on Cyprus - field evidences and ^{14}C dating results. *Z. Geomorphol.*, **46**, 19–34.

Kelletat, D., **Scheffers, A.** and **Scheffers, S.R.** (2004) Holocene tsunami deposits on the Bahaman islands of Long Island and Eleuthera. *Zeitschrift fur Geomorphologie*, **48**, 519–540.

Kelletat, D., **Whelan, F.**, **Bartel, P.** and **Scheffers, A.** (2005) New Tsunami evidences in Southern Spain Cabo de Trafalgar and Majorca Island. In: *Geomorfologia Litoral I Quarternari* (Eds E. Sanjaume and J.F. Matheu), pp. 215–222. Homenatge al professor Vincenç M. Rosselló i Verger, Universitat de València, València.

Kelletat, D., **Scheffers, S.R.** and **Scheffers, A.** (2007) Field signatures of the S-E Asian mega-tsunami along the West Coast of Thailand compared to Holocene Paleo-Tsunami from the Atlantic region. *Pure Appl. Geophys.*, **164**, 413–431.

Lamarche, G., **Pelletier, B.** and **Goff, J.** (2010) Impact of the 29 September 2009 South Pacific tsunami on Wallis and Futuna. *Mar. Geol.*, **271**, 297–302.

Lario, J., **Bardají, T.**, **Silva, P.G.**, **Zazo, C.** and **Goy, J.L.** (2016) Improving the coastal record of tsunamis in the ESI-07 scale: Tsunami Environmental Effects Scale (TEE-16 scale). *Geol. Acta*, **14**, 179–193.

Lario, J., **Spencer, C.**, **Bardají, T.**, **Marchante, A.**, **Garduño-Monroy, V.H.**, **Macias, J.** and **Ortega, S.** (2017) An Extreme Wave Event in eastern Yucatán, Mexico: evidence of a paleotsunami event during the Mayan times. In: *Proceedings of the 8th International INQUA Meeting on Paleoseismology, Active Tectonics and Archeoseismology* (Ed. GNS Science, New Zeland.), GNS Science Miscellaneous Series, **110**, 38–41.

Lau, A., **Terry, J.P.**, **Ziegler, A.**, **Pratap, A.** and **Harris, D.** (2018) Boulder emplacement and remobilisation by cyclone and submarine landslide tsunami waves near Suva City, Fiji. *Sed. Geol.*, **364**, 242–257.

López López, E.E. (2011) *Análisis de las pérdidas en México generadas por fenómenos hidrometerológicos históricos*. Tesis Licenciatura, Facultad de Ingeniería, UNAM, México, 76 pp.

Macías, J., **Mercado, A.**, **González-Vida, J.M.**, **Ortega, S.** and **Castro, M.J.** (2016) Comparison and numerical performance of Tsunami-HySEA and MOST models for LANTEX 2013 scenario. Impact assessment on Puerto Rico coasts. *Pure Appl. Geophys.*, **173**, 3973–3997.

Macías, J., **Castro, M.J.**, **Ortega, S.**, **Escalante, C.** and **González-Vida, J.M.** (2017) Performance benchmarking of Tsunami-HySEA model for NTHMP's inundation mapping activities. *Pure Appl. Geophys.*, **174**, 3147–3183.

Maouche, S., **Morhange, C.** and **Meghraoui, M.** (2009) Large boulder accumulation on the Algerian coast evidence tsunami events in the western Mediterranean. *Mar. Geol.*, **262**, 96–104.

Márquez-Azua, B., **Cabral-Cano, E.**, **Correa-Mora, F.** and **De Mets, C.** (2004) A model for Mexican neotectonics based on nationwide GPS measurements, 1993–2001. *Geofis. Int.*, **43**, 319–330.

Mastronuzzi, G. and **Sansò, P.** (2000) Boulders transport by catastrophic waves along the Ionian coast of Apulia (Southern Italy). *Mar. Geol.*, **170**, 93–103.

Mastronuzzi, G. and **Sansò, P.** (2004) Large boulder accumulations by extreme waves along the Adriatic coast of southern Apulia (Italy). *Quat. Int.*, **120**, 173–184.

Mastronuzzi, G., **Pignatelli, C.** and **Sansò, P.** (2006) Boulder fields: a valuable morphological indicator of paleotsunami in the Mediterranean Sea. *Z. Geomorph. NF Suppl.*, **146**, 173–194.

Mastronuzzi, G., **Pignatelli, C.**, **Sansò, P.** and **Selleri, G.** (2007) Boulder accumulations produced by the 20th February 1743 tsunami along the coast of South Eastern Salento (Apulia region, Italy). *Mar. Geol.*, **242**, 191–205.

May, S.M., **Willershäuser, T.** and **Vött, A.** (2010) Boulder transport by high-energy wave events at Cap Bon (NE Tunisia). *Coast. Rep.*, **16**, 1–10.

McCloskey, T.A. and **Liu, K.-B.** (2013) A 7000-year record of paleohurricane activity from a coastal wetland in Belize. *Holocene*, **23**, 278–291.

Medina, F., **Mhammdi, N.**, **Chiguer, A.**, **Akil, M.** and **Jaaidi, E.** (2011) The Rabat and Larache boulder fields; new examples of high-energy deposits related to storms and tsunami waves in north-western Morocco. *Nat. Hazards*, **59**, 725–747.

Medina-Elizalde, M., **Polanco-Martínez, J.M.**, **Lases-Hernandez, F.**, **Bradley, R.** and **Burns, S.** (2016) Testing the "tropical storm" hypothesis of Yucatán Peninsula climate variability during the Maya Terminal Classic Period. *Quatern. Res.*, **86**, 111–119.

Meza-Padilla, R., **Appendini, C.M.** and **Pedrozo-Acuña, A.** (2015) Hurricane-induced waves and storm surge modeling for the Mexican coast. *Ocean Dyn.*, **65**, 1199–1211.

Mhammdi, N., **Medina, F.**, **Kelletat, D.**, **Ahmamou, M.** and **Aloussi, L.** (2008) Large boulders along the Rabat coast (Morocco); possible emplacement by the November 1st, 1755 a.d. tsunami. *Sci. Tsunami Hazard*, **27**, 17–30.

Miller, S., **Rowe, D.A.**, **Brown, L.** and **Mandal, A.** (2014) Wave-emplaced boulders: implications for development of ''prime real estate'' seafront, North Coast Jamaica. *Bull. Eng. Geol. Environ.*, **73**, 109–122.

Morton, R.A., **Richmond, B.M.**, **Jaffe, B.E.** and **Gelfenbaum, G.** (2006) Reconnaissance investigation of Caribbean extreme wave deposits – preliminary observations, interpretations, and research directions. USGS Open-File Report 2006-1293, US Geological Survey, 41 pp.

Morton, R.A., **Richmond, B.M.**, **Jaffe, B.E.** and **Gelfenbaum, G.** (2008) Coarse-clast ridge complexes of the Caribbean: a preliminary basis for distinguishing tsunami and storm-wave origins. *J. Sediment. Res.*, **78**, 624–637.

Nandasena, N.A.K., **Paris, R.** and **Tanaka, N.** (2011a) Reassessment of hydrodynamic equations: minimum flow velocity to initiate boulder transport by high energy events (storms, tsunamis). *Mar. Geol.*, **281**, 70–84.

Nandasena, N.A.K., **Paris, R.** and **Tanaka, N.** (2011b) Numerical assessment of boulder transport by the 2004 Indian ocean tsunami in Lhok Nga, West Banda Aceh (Sumatra, Indonesia). *Comput. Geosci.*, **37**, 1391–1399.

Nandasena, N.A.K., **Sasaki, Y.** and **Tanaka, N.** (2012) Modeling field observations of the 2011 Great East Japan tsunami: efficacy of artificial and natural structures on tsunami mitigation. *Coast. Eng.*, **67**, 1–13.

Nandasena, N.A.K., **Tanaka, N.**, **Sasaki, Y.** and **Osada, M.** (2014) Reprint of "Boulder transport by the 2011 Great East Japan tsunami: comprehensive field observations and whither model predictions?" *Mar. Geol.*, **358**, 49–66.

Noormets, R., **Crook, K.A.W.** and **Felton, E.A.** (2004) Sedimentology of rocky shorelines: 3. Hydrodynamics of megaclast emplacement and transport on a shore platform, Oahu, Hawaii. *Sed. Geol.*, **172**, 41–65.

Nott, J. (1997) Extremely high-energy wave deposits inside the Great Barrier Reef, Australia: determining the cause - tsunami or tropical cyclone. *Mar. Geol.*, **14**, 193–207.

Nott, J. (2003) Waves, coastal boulder deposits and the importance of the pretransport setting. *Earth Planet. Sci. Lett.*, **210**, 269–276.

Nott, J. (2004) The tsunami hypothesis: comparisons of the field evidence against the effects, on the Western Australian coast, of some of the most powerful storms on Earth. *Mar. Geol.*, **208**, 1–12.

Paris, R., **Wassmer, P.**, **Sartohadi, J.**, **Lavigne, F.**, **Barthomeuf, B.**, **Desgages, E.**, **Grancher, D.**, **Baumert, P.**, **Vautier, F.**, **Brunstein, D.** and **Gomez, C.** (2009) Tsunamis as geomorphic crises: lessons from the December 26, 2004 tsunami in Lhok Nga, west Banda Aceh (Sumatra, Indonesia). *Geomorphology*, **104**, 59–72.

Paris, R., **Fournier, J.**, **Poizot, E.**, **Etienne, S.**, **Morin, J.**, **Lavigne, F.** and **Wassmer, P.** (2010) Boulder and fine sediment transport and deposition by the 2004 tsunami in Lhok Nga (western Banda Aceh, Sumatra, Indonesia): a coupled offshore–onshore model. *Mar. Geol.*, **268**, 43–54.

Pignatelli, C., **Sanso, P.** and **Mastronuzzi, G.** (2009) Evaluation of tsunami flooding using geomorphologic evidence. *Mar. Geol.*, **260**, 6–18.

Richmond, B.M., **Buckley, M.**, **Etienne, S.**, **Chagué-Goff, C.**, **Clark, K.**, **Goff, J.**, **Dominey-Howes, D.** and **Strotz, L.** (2011) Deposits, flow characteristics, and landscape change resulting from the September 2009 South Pacific tsunami in the Samoan islands. *Earth Sci. Rev.*, **107**, 38–51.

Rixhon, G., **May, S.M.**, **Engel, M.**, **Mechernich, S.**, **Schroeder-Ritzrau, A.**, **Frank, N.**, **Fohlmeister, J.**, **Boulvain, F.**, **Dunai, T.** and **Brückner, H.** (2018) Multiple dating approach (^{14}C, $^{230}Th/U$ and ^{36}Cl) of tsunami-transported reef-top boulders on Bonaire (Leeward Antilles) - Current achievements and challenges. *Mar. Geol.*, **396**, 100–113.

Rizza, M., **Ritz, J.F.**, **Braucher, R.**, **Vassallo, R.**, **Prentice, C.**, **Mahan, S.**, **McGill, S.**, **Chauvet, A.**, **Marco, S.**, **Todbileg, M.**, **Demberel, S.** and **Bourlès, D.** (2011) Slip rate and slip magnitudes of past earthquakes along the Bogd left-lateral strike-slip fault (Mongolia). *Geophys. J. Int.*, **186**, 897–927.

Rodríguez-Pascua, M.A., **Pérez-López, R.**, **Silva, P.G.**, **Giner-Robles, J.L.**, **Garduño-Monroy, V.H.** and **Reicherter, K.** (2011) A comprehensive classification of Earthquake Archaeological Effects (EAE) for Archaeoseismology. *Quatern. Int.*, **242**, 20–30.

Roig-Munar, F.X., **Vilaplana, J.M.**, **Rodriguez-Perea, A.**, **Martín-Prieto, J.A.** and **Gelabert, B.** (2018) Tsunamis boulders on the rocky shores of Minorca (Balearic Islands). *Nat. Hazards Earth Syst. Sci.*, **18**, 1985–1998.

Rosengaus Moshinsky, M. and **Sánchez Sesma, J.** (1990) Gilbert: ejemplo de huracanes de gran intensidad. *Ingeniería Hidráulica en México*, **1**, 13–36.

Rosengaus Moshinsky, M., **Jiménez Espinosa, M.** and **Vázquez Conde, M.T.** (2014) *Atlas climatológico de ciclones tropicales en México*. CENAPRED, México, 108 pp.

Scheffers, A. (2006) Sedimentary impacts of Holocene tsunami events from the intraAmerican seas and southern Europe. *Z. Geomorphol.*, **146**, 7–37.

Scheffers, A. and **Kinis, S.** (2014) Stable imbrication and delicate/unstable settings in coastal boulder deposits: Indicators for tsunami dislocation? *Quatern. Intern.*, **332**, 73–84.

Scheffers, A., **Scheffers, S.** and **Kelletat, D.** (2005) Paleo-tsunami relics on the Southern and Central Antillean Island Arc (Grenada, St. Lucia and Guadeloupe). *J. Coastal Res.*, **21**, 263–273.

Scheffers, A., **Kelletat, D.**, **Vött, A.** and **May, S.M.** (2008a) Late Holocene tsunami traces on the western and southern coastlines of the Peloponnesus (Greece). *Earth Planet. Sci. Lett.*, **269**, 271–279.

Scheffers, S., **Scheffers, A.**, **Kelletat, D.** and **Bryant, E.** (2008b) The Paleo-tsunami history of west Australia. *Earth Planet. Sci. Lett.*, **270**, 137–146.

Scheffers, S.R., **Haviser, J.**, **Browne, T.** and **Scheffers, A.** (2009) Tsunamis, hurricanes, the demise of coral reefs and shifts in prehistoric human populations in the Caribbean. *Quatern. Intern.*, **195**, 69–87.

Scheffers, A., **Kelletat, D.**, **Haslett, S.K.**, **Scheffers, S.** and **Browne, T.** (2010) Coastal boulder deposits in Galway Bay and the Aran islands, western Ireland. *Z. Geomorphol.*, **54**, 247–279.

Scheffers, A.M., **Engel, M.**, **May, S.M.**, **Scheffers, S.R.**, **Joannes-Boyau, R.**, **Hänssler, E.**, **Kennedy, K.**, **Kelletat, D.**, **Brückner, H.**, **Vött, A.**, **Schellmann, G.**, **Schäbitz, F.**, **Radtke, U.**, **Sommer, B.**, **Willershäuser, T.** and **Felis, T.** (2014) Potential and limits of combining studies of coarse- and fine-grained sediments for the coastal event history of a Caribbean carbonate environment. In: *Sedimentary Coastal Zones from High to Low Latitudes: Similarities and Differences* (Ed. I.P. Martini) Geol. Soc. London Spec. Pub, **388**, 503–531.

Schneirder, B., **Hoffman, G.**, **Falkenroth, M.** and **Grade, J.** (2018) Tsunami and storm sediments in Oman: Characterizing extreme wave deposits using terrestrial laser scanning. *J. Coast. Conserv.* https://doi.org/10.1007/s11852-018-0663-4

Shah-hosseini, M., **Morhange, C.**, **Naderi Beni, A.**, **Marriner, N.**, **Lahijani, H.**, **Hamzeh, M.** and **Sabatier, F.** (2011)

Coastal boulders as evidence for high-energy waves on the Iranian coast of Makran. *Mar. Geol.*, **290**, 17–28.

Shaw, C.E. and **Benson, L.** (2015) Possible tsunami deposits on the Caribbean coast of the Yucatán peninsula. *J. Coastal Res.*, **31**, 1306–1316.

Spiske, M. and **Bahlburg, H.** (2011) A quasi-experimental setting of coarse clast transport by the 2010 Chile tsunami (Bucalemu, Central Chile). *Mar. Geol.*, **289**, 72–85.

Spiske, M., **Böröcz, Z.** and **Bahlburg, H.** (2008) The role of porosity in discriminating between tsunami and hurricane emplacement of boulders - A case study from the Lesser Antilles, southern Caribbean. *Earth Planet. Sci. Lett.*, **268**, 384–396.

SSN (2018) *Catálogo de Sismos*. Servicio Sismológico Nacional, México. http://www2.ssn.unam.mx:8080/catalogo/ (last conexión 14-02-2018).

Switzer, A.D. and **Burston, J.M.** (2010) Competing mechanisms for boulder deposition on the southeast Australian coast. *Geomorphology*, **114**, 42–54.

Szabo, B.J., **Ward, W.C.**, **Weidie, A.E.** and **Brady, M.J.** (1978) Age and magnitude of the late Pleistocene sea-level rise on the eastern Yucatán Peninsula. *Geology*, **6**, 713–715.

Terry, J.P., **Lau, A.Y.A.** and **Etienne, S.** (2013) *Reef-Platform Coral Boulders - Evidence for High-Energy Marine Inundation Events on Tropical Coastlines*. Springer, Singapore, 105 pp.

USGS (2018) Earthquake Catalog (online). Available at: https://earthquake.usgs.gov/earthquakes/search/.

Vött, A. and **May, S.M.** (2009) Auf den Spuren von Tsunamis im östlichen Mittelmeer. *Geogr. Rundsch.*, **12**, 42–48.

Vött, A., **Lang, F.**, **Bruckner, H.**, **Gakipapanastassiou, K.**, **Maroukian, H.**, **Papanastassiou, D.**, **Giannikos, A.**, **Hadler, H.**, **Handl, M.**, **Ntageretzis, K.**, **Willershäuser, T.** and **Zander, A.** (2010) Sedimentological and geoarchaeological evidence of multiple tsunamigenic imprint on the Bay of Palairos-Pogonia (Akarnania, NW Greece). *Quat. Int.*, **242**, 213–239.

Vött, A., **Bareth, G.**, **Brückner, H.**, **Lang, F.**, **Sakellariou, D.**, **Hadler, H.**, **Ntageretzis, K.** and **Willershäuser, T.** (2011) Olympia's harbour site Pheia (Ellis, western Peleponnese, Greece) destroyed by tsunami impact. *Erde*, **142**, 259–288.

Ward, W.C. (1985) Quaternary geology of the northeastern Yucatán Peninsula. In: *Geology and Hydrogeology of the Yucatán and Quaternary Geology of the Northeastern Yucatán Peninsula* (Eds W.C. Ward, A.E. Weidie and W. Back), pp. 23–53. New Orleans Geological Society, New Orleans, LA.

Weidie, A.E. (1985) Geology of the Yucatán Platform. In: *Geology and Hydrogeology of the Yucatán and Quaternary Geology of the Northeastern Yucatán Peninsula* (Eds W.C. Ward, A.E. Weidie and W. Back), pp. 1–19. New Orleans Geological Society, New Orleans, LA.

Whelan, F. and **Kelletat, D.** (2002) Geomorphic evidence and relative and absolute dating results for tsunami events on Cyprus. *Sci. Tsunami Hazard*, **20**, 3–18.

Whelan, F. and **Kelletat, D.** (2003). Analysis of tsunami deposits at Cabo de Trafalgar, Spain, using GIS and GPS technology. In: *Neue Ergebnisse der Küsten und Meeresforschung* (Eds D. Kelletat), Essener Geographische Arbeiten, Essen, **35**, 11–25.

Whelan, F. and **Kelletat, D.** (2005) Boulder Deposits on the Southern Spanish Atlantic Coast: Possible Evidence for the 1755 AD Lisbon Tsunami? *Sci. Tsunami Hazard*, **23**, 25–38.

Yamada, M., **Fujino, S.** and **Goto, K.** (2014) Deposition of sediments of diverse sizes by the 2011 Tohoku-oki tsunami at Miyako City, Japan. *Mar. Geol.*, **358**, 67–78.

Zúñiga, I. (2016) Arquitectura Costa Oriental de Quintana Roo: un legado de Postclásico Tardío en el Caribe mexicano. *Memorias, Revista Digital de Arqueología e Historia desde el Caribe*, **29**, 136–166.

Manuscript received 12 March 2018; revision accepted 1 July 2019